nature communications

Article

https://doi.org/10.1038/s41467-025-61681-6

A genetically tractable non-vertebrate system to study complete camera-type eye regeneration

Received: 10 July 2024

Accepted: 26 June 2025

Published online: 06 August 2025

Check for updates

Alice Accorsi[1,2] ✉, Brenda Pardo[1,3], Eric Ross[1], Timothy J. Corbin[1], Melainia McClain[1], Kyle Weaver[1], Kym Delventhal[1,4], Asmita Gattamraju[2], Jason A. Morrison[1], Mary Cathleen McKinney[1], Sean A. McKinney[1] & Alejandro Sánchez Alvarado[1,5] ✉

Camera-type eyes are complex sensory organs susceptible to irreversible damage. Their repair is difficult to study due to the paucity of camera-type eye regeneration models. Identifying a genetically tractable organism with the ability to fully regenerate complete camera-type eyes would help overcome this difficulty. Here, we introduce the apple snail *Pomacea canaliculata*, capable of full regeneration of camera-type eyes even after complete resection. We defined anatomical components of *P. canaliculata* eyes and genes expressed during crucial steps of their regeneration. By exploiting the unique features of this organism, we successfully established stable mutant lines in apple snails. Our studies reveal that, akin to humans, *pax6* is indispensable for eye development in apple snails, establishing this as a research organism to unravel the mechanisms of camera-type eye regeneration. This work expands our understanding of complex sensory organ regeneration and offers a way to explore this process.

The proper functioning of organs is intricately tied to their embryonic development, a complex and stereotypical multi-step process involving tissue organization and cell differentiation in the context of whole-body development. Post-embryogenesis, many animals lose the ability to fully regenerate new organs, some retain regenerative capacities within certain tissue or age and others exhibit remarkable abilities, regenerating entire organisms from small body portions[1,2]. Regeneration involves steps such as wound healing, detection of missing structures, activation of cell proliferation, determination of anatomical patterning, growth and integration of new tissues into the existing body[1,2]. Despite numerous studies on mechanisms driving regeneration in different organisms and tissues, many questions persist about the key features of a regeneration-permissive environment.

Eyes serve as fundamental sensory organs for numerous species, enabling exploration and interaction with their environments. The camera-type eye stands out as a complex and highly specialized organ, seemingly eluding complete regeneration after full resection resulting in irreversible loss of this organ after injury or damage. Camera-type eyes are capable of high-resolution image formation and are characterized by a single closed chamber, a lens, a cornea and a retina housing numerous photoreceptor cells equipped with molecular machinery for light detection. Examples of these can be found in human and more broadly in vertebrates, and among spiders and mollusks[3–5]. Camera-type eyes are just one of the eye types present among metazoans. The pigmented cup is a non-image-forming eye type, featured by planarians and distinguished by a cup housing photoreceptors and filled with dark pigments[3–5]. Bivalves, insects and decapods are examples of organisms with compound eyes, which result from several smaller units known as ocelli organized into a larger organ[3–5].

[1]Stowers Institute for Medical Research, Kansas City, MO, USA. [2]Department of Molecular and Cellular Biology, University of California, Davis, CA, USA. [3]Present address: Department of Cell Biology, Duke University, Durham, NC, USA. [4]Present address: HHMI Janelia Research Campus, Ashburn, VA, USA. [5]Present address: Howard Hughes Medical Institute, Chevy Chase, MD, USA. ✉e-mail: aaccorsi@ucdavis.edu; asa@stowers.org

In the past, research on eye regeneration has predominantly concentrated on complete regrowth of simpler planarian pigmented cups[6] and on partial regeneration of camera-type eyes in vertebrates with robust regenerative abilities, such as fishes, newts and frogs[7–10]. These remarkable animals can repair specific components following minor injuries, such as lens or retinal cell ablations, through the activation of the ciliary marginal zone or of Müller glial cells residing in the mature retina[7,9,10]. While these studies have significantly enhanced our understanding of eye regeneration, a mechanistic comprehension of complete adult camera-type eye regeneration remains elusive.

To overcome the existing limitation and expand our understanding of visual system regeneration, an organism characterized by camera-type eyes, robust regenerative potential and amenability to genome manipulation would be highly advantageous. The prevalence of camera-type eyes spans various animal phyla, including cnidarians, annelids, mollusks, crustaceans, arthropods and vertebrates[3–5]. In 1766, Spallanzani described the remarkable regenerative potential of garden snails following head amputations[11]. More recently, reports indicated the ability of certain gastropods to regenerate their visual systems[12–14]. These initial findings suggest gastropods could be useful organisms for investigating complete camera-type eye regeneration. Thus, we focused on developing a gastropod model amenable to genome manipulation[15]. *Pomacea canaliculata*, also known as the golden apple snail, is an amphibious freshwater gastropod native to South America and belonging to the *Ampullariidae* taxon[16]. These organisms exhibit resilience to diverse environmental conditions, breed throughout the year and have successfully completed their life cycle in captivity, making them an ideal organism for laboratory maintenance[16]. *P. canaliculata* is diploid[17] and both its nuclear (440 Mb) and mitochondrial genomes have been sequenced, assembled and annotated[18–20].

Here, we characterize the camera-type eye of *P. canaliculata* and describe the complete regeneration of this sensory organ after complete amputation. We also report on methods for collecting and microinjecting zygotes and for culturing embryos. These protocols allowed us to introduce CRISPR-Cas9 technology to edit the apple snail genome and obtain stable mutant lines in *P. canaliculata*. Finally, we show that *pax6* function in eye development has been conserved in apple snails by developing the first *pax6*$^{-/-}$ lophotrochozoan. This work opens the door to studying the function of genes potentially involved in camera-type eye regeneration in this, now genetically tractable, organism.

Results

P. canaliculata has complex camera-type eyes

Camera-type eyes are present in vertebrates and characterized by one closed chamber with the light traveling through a transparent cornea, an anterior chamber, a lens, a posterior chamber and multiple retina layers to finally reach the apical part of the photoreceptors, also called the outer segment[3–5]. The outer segment of the photoreceptors is an area where the visual pigments, molecules that activate a signaling cascade when hit by photons, are hosted on the membranes[21,22]. Camera-type eyes can also be found in invertebrate organisms such as mollusks and specifically cephalopods as well as some gastropods, such as the tiger conch, *Conomurex luhuanus*[3–5,23].

With the goal of finding an organism with camera-type eyes and high regenerative potential, we sought to determine if the apple snail *P. canaliculata* had camera-type eyes suitable for study (see Fig. 1A). The *P. canaliculata* eye bulb is located on top of a short eye stalk and the cornea is a circular transparent epithelium on its apical part (see Fig. 1B). Through micro-dissection, the retina with the enclosed lens can be isolated. The black pigmentation of the retina is uniformly distributed except for a circular area on its anterior side, which is not pigmented to allow for the transmission of the light (see Fig. 1C). The white optic nerve moves from the posterior side of the retina, through the eye stalk and reaches to the cerebral ganglia. The lens of *P. canaliculata* is oval and completely transparent and, through it, we can observe in-focus, sharp, inverted images, similar to the vertebrate lenses (see Fig. 1D).

Longitudinal sections of the *P. canaliculata* eye show the presence of a cornea, an anterior chamber filled with loose extracellular matrix, a thin layer of unpigmented cells and the posterior chamber, delimited by the retina and mostly occupied by the lens (see Fig. 1E, F and Supplementary Fig. 1A–D). Ultra-structurally, the lens looks homogeneous in its composition (see Fig. 1G and Supplementary Fig. 1D).

The most abundant cells in the apple snail retina are rhabdomeric photoreceptors, a type of photoreceptor more prevalent among invertebrates and with microvilli in their outer segment (see Fig. 1E, H and Supplementary Fig. 1D–F). The photoreceptor apices, or outer segments, face the lens, similar to cephalopods. A layer of cytoplasmic dark pigment granules is localized between the outer and inner segment of the photoreceptors, providing directional information and protection of deeper tissues from UV light (see Fig. 1E, I). The photoreceptor cytoplasm is filled with small and homogeneous photic vesicles and more rarely with mitochondria and ribosomes (see Fig. 1J). The photoreceptor nuclei are basal, close to the neuropile or bundles of axons that move posteriorly to form the optic nerve (see Fig. 1E). In this basal region, we observed synapses between the basal part of the photoreceptors and axons, containing morphologically heterogeneous vesicles, larger and more electron-dense than the photic vesicles (see Fig. 1K and Supplementary Fig. 1K). Additionally, we found several ciliated cells in multiple areas of the retina, such as intercalated in the microvilli and closer to the basal part of the photoreceptors (see Supplementary Fig. 1G–I). Finally, the eye bulb is surrounded by connective tissue, muscle tissue and extracellular matrix (see Fig. 1E and Supplementary Fig. 1J).

We conclude that *P. canaliculata* has complex camera-type eyes, that share some anatomical features with vertebrate eyes and others with camera-type eyes previously described in invertebrates, such as cephalopods and other gastropods.

P. canaliculata genome has genes expressed in vertebrate camera-type eye

Eyes are complex organs and a full consensus about their evolutionary history has not been reached. One of the main challenges is represented by the fact that the consideration of different elements, such as anatomy, cell types or gene expression might direct us towards different conclusions. While vertebrate and cephalopod eyes have historically been used as an example of convergent evolution mainly based on their anatomical structure, more recent studies in cellular and molecular biology support hypotheses of parallel evolution[24,25]. Specifically, in camera-type eyes from both vertebrate and cephalopods, genes such as *pax6*, *vsx* and *rx* have a conserved function in eye development[26–28].

We first looked at the overlap between the genes present in *P. canaliculata* genome and those assigned to GO terms related to "visual system" in human (a vertebrate with camera-type eyes) and/or the fruit fly *Drosophila melanogaster* (an invertebrate with compound eyes) (see Fig. 1L). Interestingly, the group of genes shared between apple snails and humans is enriched with those involved in the overall morphogenesis of the camera-type eye and of its individual components, such as the development or formation of cornea, lens, photoreceptors and retina layers. The group of genes shared between apple snails and flies is enriched with those involved more specifically in the fly photoreceptor development. We observed genes shared between all the three animals to a lesser extent (see Fig. 1M and Supplementary Data 1).

Additionally, we took advantage of the previously published vertebrate Gene Regulatory Networks (GRNs) driving optic cup patterning, camera-type eye morphogenesis and retina cell differentiation

https://doi.org/10.1038/s41467-025-61681-6

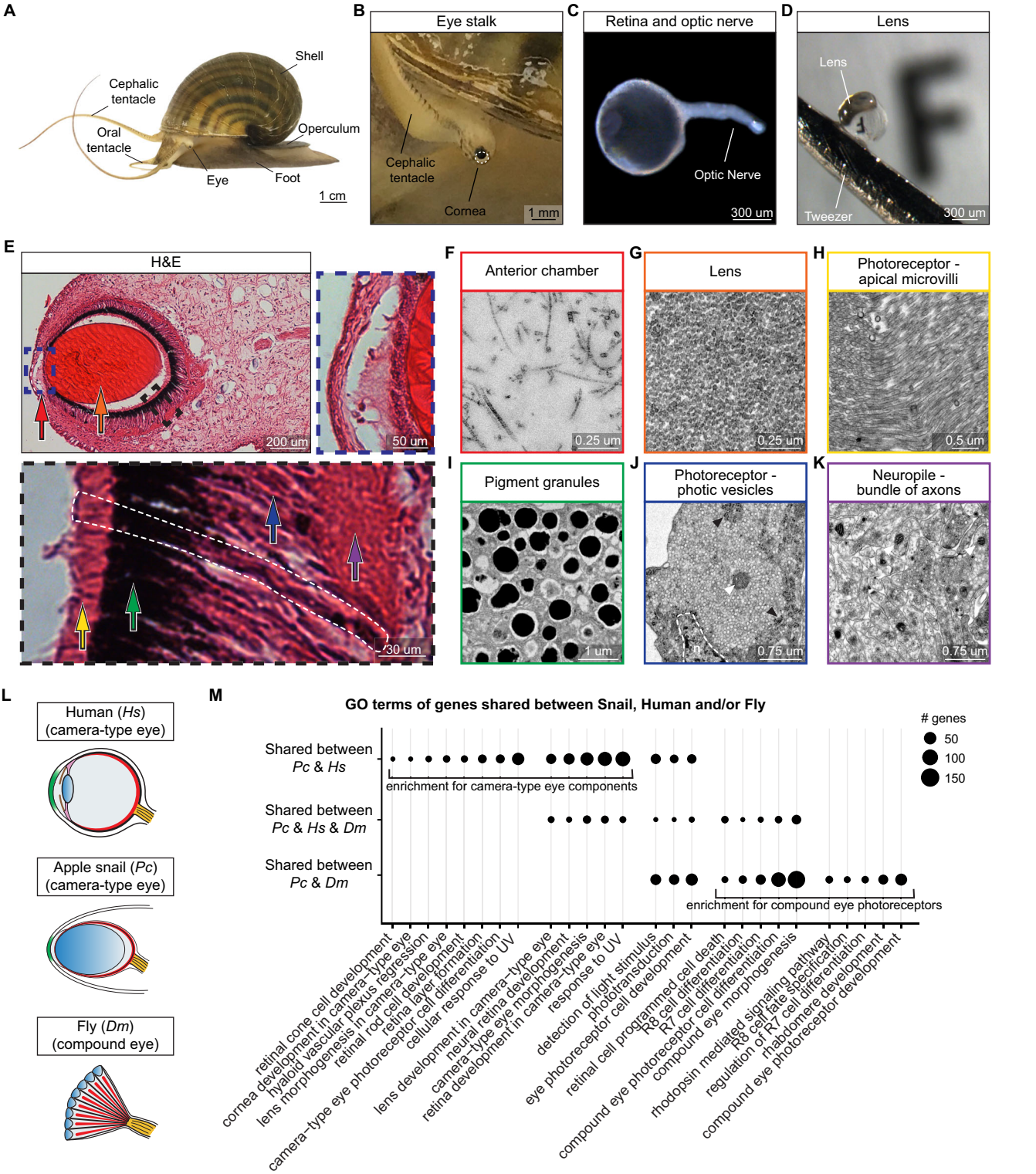

and looked for their in silico orthologs in *P. canaliculata* (see Supplementary Fig. 1L, M and Supplementary Data 2). We found 62% of these genes in the apple snail genome and for an additional 29% of these genes we found genes belonging to the broader gene family (see Supplementary Data 2).

Together, our analyses demonstrate that the apple snail genome includes several genes involved in the development of the vertebrate camera-type eye and its individual components. Additionally, *P. canaliculata* also has genes usually associated with *D. melanogaster* rhabdomeric photoreceptors. We can conclude that *P. canaliculata* shares molecular similarities with both vertebrate camera-type eyes and with invertebrate photoreceptors.

P. canaliculata camera-type eyes can fully regenerate after complete amputation

To test if *P. canaliculata* can fully regenerate its camera-type eyes, we completely amputated the eye stalk, removing all eye bulb components (see Supplementary Fig. 2A). Strikingly, we observed complete regeneration of the eye bulb and eye stalk within a month (see Fig. 2A). To characterize morphological changes and cell proliferation, we

Fig. 1 | *P. canaliculata* has complex camera-type eyes. A Adult *P. canaliculata*. **B** Eye bulb and eye stalk with cornea (dashed line). **C** Isolated optic nerve and retina with the lens enclosed in it. **D** Isolated lens held with tweezers in front of a paper with the letter F printed in font size 5. **E** Hematoxylin and eosin (H&E) staining of *P. canaliculata* eye longitudinal sections. Cornea (dashed line on the left), anterior chamber (red arrow), lens (orange arrow), posterior chamber, retina, optic nerve and surrounding connective tissue, muscle tissue and extracellular matrix (ECM) can be distinguished. The 2 insets highlight the cornea and the anterior part of the lens (blue dashed line) and a portion of the retina (black dashed line). In the latter, a photoreceptor (white dashed line), the photoreceptor outer segments (yellow arrow), pigment granules (green arrow), photoreceptor inner segments (blue arrow) and neuropile (purple arrow) are shown. Arrows in (**E**) and images in (**F**–**K**) have the same color-code. TEM images of **(F)** anterior chamber filled with ECM; **G** lens with a densely packed structure; **H** outer segment of rhabdomeric photoreceptors characterized by microvilli; **I** pigment granules; **J** densely packed photic vesicles occupy an extensive portion of the photoreceptor cytoplasm together with rare mitochondria (white arrowhead) and ribosomes (black arrowheads), n nucleus; **K** neuropile, or bundle of axons forming the optic nerve, filled with heterogeneous vesicles. The images showed in (**E**–**K**) are representative of data collected through three independent experiments. **L** Schematic representation of eye anatomy for human (*Hs*), apple snail (*Pc*) and *Drosophila* (*Dm*). **M** Gene Ontology (GO) enrichment analysis of *P. canaliculata* (*Pc*) genes bioinformatically defined as orthologs of human (*Hs*) and/or fly (*Dm*) genes. For this analysis only GO terms related to eye development and function were taken into consideration. The plot shows the number of genes for each GO term that can be found in both snail and human but not in fly (first row), in snail, human and fly (middle row), or in snail and fly but not in human (last row). Adjusted *p* value cutoff of 1e−5. Manually selected representative terms (see Supplementary Fig. 1 and Supplementary Data 1).

performed a time course of Hematoxylin and Eosin (H&E) staining as well as an anti-Phospho-Histone H3 (anti-H3P) antibody staining and 24 h BrdU pulse chase experiment.

We identified four main stages of eye regeneration in *P. canaliculata*: wound healing, blastema formation, retina and lens emergence and eye components maturation. The wound completely heals in the first 24 h, concurrent with a significant increase of H3P positive cells (see Fig. 2B and Supplementary Fig. 2B, C). The blastema, tissue composed of loose proliferating cells and developed by several animals during the regeneration process[1,2], forms at 3 and 6 days post amputation (dpa) (see Fig. 2C, F and Supplementary Fig. 2B, C). The new optic cup, invagination of retinal cell precursors organized in a cup that closes on itself, develops at 9 dpa. This optic cup is localized close to the apical portion of the eye stalk and already presents some black pigmentation (see Fig. 2D). At 12 dpa the regenerating retina is well defined with the lens developing inside it (see Fig. 2D). All the major morphological features of the eye bulb are present by 15 dpa, including the optic nerve (see Fig. 2E). At later time points (21 and 28 dpa) all these anatomical components continue to mature and grow (see Fig. 2E).

We determined the growth rate of the regenerating eye by calculating the eye bulb area and found that at 28 dpa it is still significantly smaller than the one of the original eye (see Fig. 2G). Interestingly, we observed the different components (lens, photoreceptor microvilli, pigment granules, photoreceptor inner segment and neuropile) do not form simultaneously and do not grow at the same rate. Specifically, the photoreceptor inner segment occupies a significant percentage of the eye bulb at 12 and 15 dpa and grows less over time compared to the other layers. By 28 dpa, the relative sizes of these components become similar to those observed in the intact eyes (see Fig. 2H and Supplementary Fig. 2D–H).

Altogether, these data show that *P. canaliculata* fully regenerates its camera-type eyes, healing the wound in the first 24 h and forming a blastema from 3 to 6 dpa. Intense cell proliferation accompanies retina emergence through the formation of an optic cup. After lens emergence at 12 dpa, there is a phase of maturation and growth of the eye components through cell proliferation and retinal layer differentiation.

P. canaliculata regenerating eyes express genes driving vertebrate eye development

Following our morphological characterization, we next wanted to evaluate the changes in gene expression during *P. canaliculata* eye regeneration. We generated bulk transcriptomes at morphologically defined regeneration time points (see Fig. 3A and Supplementary Fig. 3A). As expected, the segregation of the samples in the MDS plot mirrors morphology showing that the early time points of regeneration (1 and 3 dpa) are transcriptionally the most different from the intact eyes (largest distance in Dimension 1) while the later time points (21 and 28 dpa) are the closest to the intact eyes (see Fig. 3B). All time points are chronologically positioned in an arc shape from 1 to 28 dpa with the peak at 6 dpa (highest distance in Dimension 2) (see Fig. 3B).

To further dissect the molecular dynamics of snail eye regeneration, we calculated the number of differentially expressed (DE) genes between the regeneration time points and the intact eye. While initially there are about 9000 DE genes, this number steadily decreases until 28 dpa where there are 468 genes up-regulated and 707 genes down-regulated compared to the intact eye (see Fig. 3C and Supplementary Fig. 3B, C). To gain a better understanding of the steps followed by the regeneration process, GO term enrichment analysis and heatmaps were performed on DE genes (see Fig. 3D, E and Supplementary Fig. 4 and Supplementary Data 3). We found an enrichment of genes involved in wound healing and cell migration in the first 24 h after amputation. Genes related to DNA replication and regulation of the cell cycle were up-regulated at 3 dpa and persisted throughout the regeneration time points. At 3 and 6 dpa genes associated with neurogenesis, axon guidance and camera-type eye development are already enriched and up-regulated. Enrichment for the detection of visible light and photoreceptor activities starts at 12 dpa, while a molecular signature for phototransduction and visual perception happens later in the time course. Interestingly, terms that are enriched and expressed at a higher level in the intact eye compared to the 28 dpa are related to synaptic vesicle biology and visual pigments (see Fig. 3D, E and Supplementary Fig. 4 and Supplementary Data 3). The reduced but still significant number of differentially expressed genes between 28 dpa and intact eyes suggests the regenerating eye may require a longer time to fully complete the maturation of certain cell types.

To identify ultra-structural differences among the intact and the regenerating eyes, we analyzed the regenerating tissue at longer time points with electron microscopy. Interestingly, the main differences that we noticed throughout the time course were related to the presence of photic vesicles. At 1 month post amputation (mpa) the cytoplasm of the photoreceptors does not contain any photic vesicles, while there is abundance of ribosomes and endoplasmic reticulum (ER). Some areas with photic vesicles were found in the 2 mpa tissue, although less packed and surrounded by areas still containing ribosomes and ER. By 3 mpa the photic vesicle distribution is indistinguishable from the intact eye (see Fig. 3F). At this time point we also observed that the microvilli of the rhabdomeric photoreceptors and the cilia among the microvilli were recovered (see Fig. 3G).

Overall, these data provide a molecular blueprint of snail eye regeneration, as well as the molecular and ultra-structural differences still present between the 28 dpa and the intact eye.

P. canaliculata zygotes can be cultured *ex ovo* and microinjected with exogenous mRNA

To test gene function and investigate the molecular mechanisms driving development and regeneration of eyes in *P. canaliculata*, we sought to build tools to genetically modify these snails. Since the

https://doi.org/10.1038/s41467-025-61681-6

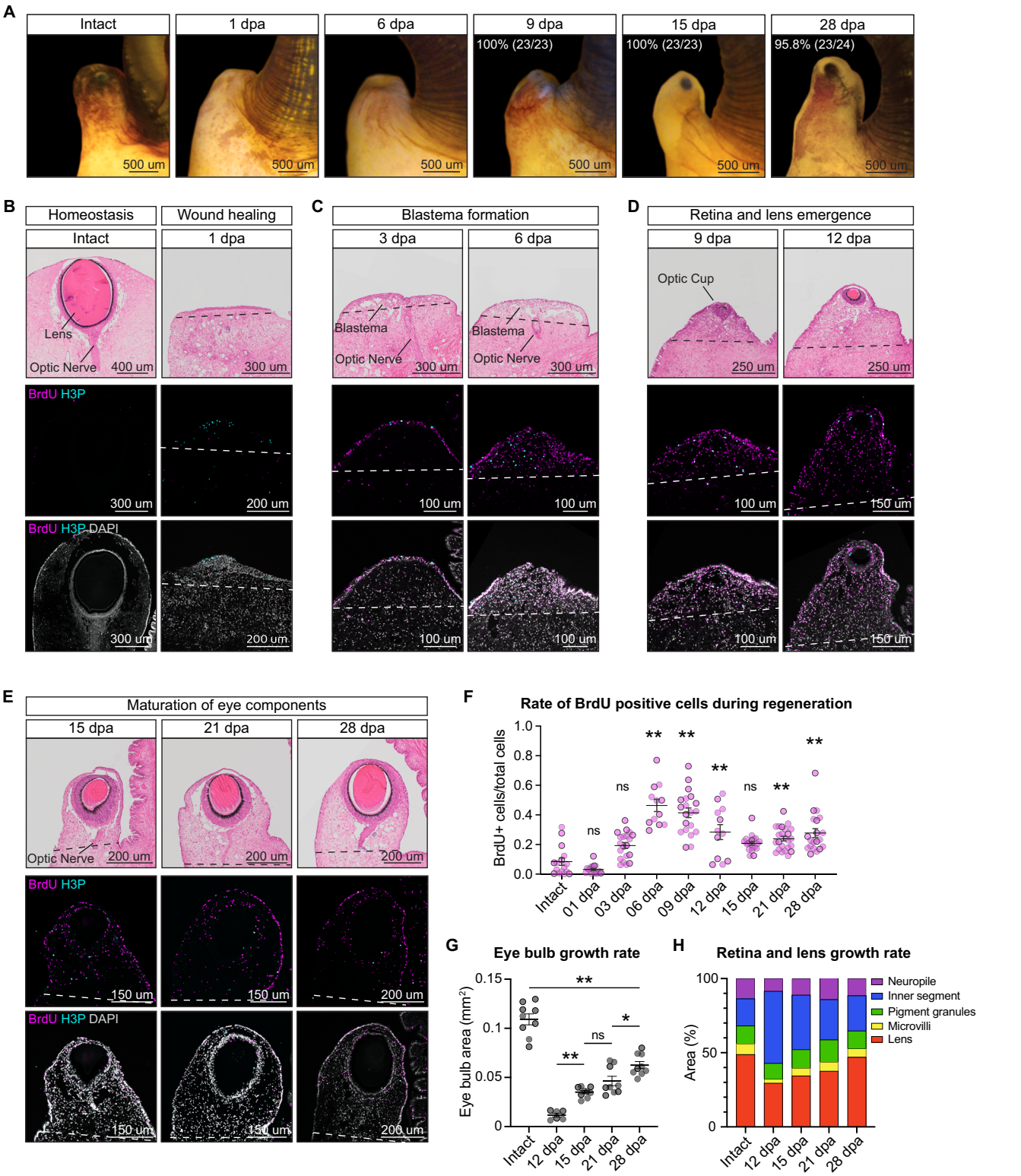

oocytes are internally fertilized, we developed a protocol to efficiently collect zygotes, opening the external capsules as soon as they are laid by the female. These embryos cannot fully develop without the pink perivitelline fluid (PVF) present inside the capsule and representing their main source of nutrients until hatching. To grow embryos after manipulations, we developed a protocol to culture them *ex ovo* in an extract of perivitelline fluid (ePVF) (see Fig. 4A). To avoid evaporation, drops of ePVF were placed in a Petri dish and covered in paraffin oil. The embryos cultured *ex ovo* complete development in 10–13 days, similarly to embryos growing in their original capsules (see Fig. 4B and Supplementary Fig. 5A). In addition to growing manipulated embryos that were removed from their capsules, this protocol now allows us, for the first time, to observe embryonic development live (see Fig. 4B and Supplementary Fig. 5A).

As apple snail zygotes are similar in size to one-cell mouse embryos (~100 um in diameter), we adopted a modified micro-injection system similar to the one used for creation of transgenic mice. This system included the standard inverted microscope, a glass

Fig. 2 | *P. canaliculata* camera-type eyes can fully regenerate after complete amputation. A Regeneration time course after complete amputation of the eye bulb. **B**–**E** Longitudinal sections of the eye stalk during eye regeneration time course stained with either H&E (top images) or anti-BrdU (magenta) and anti-H3P (cyan) (central and bottom row of images). The dashed lines represent where the cut for eye amputation was performed. BrdU and H3P positive cells where counted in the tissue above the dashed lines. **F** Quantification of BrdU positive cells in the regenerating tissue area during the eye regeneration time course. $n = 3$ snails for 6 and 12 dpa; $n = 4$ snails for Intact and 1 dpa; $n = 5$ snails for 3, 9, 15 and 28 days post amputation (dpa); $n = 6$ snails for 21 dpa; for each sample 4 sections were analyzed; non-parametric Kruskal–Wallis ANOVA with Dunn's post hoc multiple comparisons test determined statistical differences between regenerating samples and Intact eye; adjusted p values are <0.0001 for 6 and 9 dpa, 0.0035 for 12 and 21 dpa and 0.0009 for 28 dpa. **G** Quantification of the eye bulb area during the eye regeneration time course. $n = 3$ snails/time point, 3 sections each; one-way ANOVA with Tukey's post hoc multiple comparisons test determined statistical differences between samples; adjusted p values are 0.0046 for 15 vs 12 dpa, 0.0447 for 28 vs 21 dpa and <0.0001 for Intact vs 28 dpa. **H** Quantification of the relative area of the eye bulb components (lens in red, photoreceptor microvilli in yellow, pigmented layer in green, photoreceptor inner segment in blue and neuropile in purple) during the eye regeneration time course. Data are represented as mean ± SEM. $n = 3$ snails/time point, 3 sections each. *p value < 0.05, **p value < 0.01, ns non-significant (see Supplementary Fig. 2).

micro-injection needle and a glass holding pipette. In addition to this equipment, we incorporated the use of a cold microscope stage and a MICRO-ePORE pinpoint electroporation system (see Fig. 4C and Supplementary Fig. 5B, C). Multiple rounds of micro-injection were performed to further optimize equipment and reagents resulting in increasing survival rates. Using a holding pipette, a cold stage (at 12 °C), media supplemented with FBS and the MICRO-ePORE, we reached an average of 30–40% survival rate that increased to more than 65% with user experience (see Fig. 4D). Initially, we micro-injected fluorescent dextran and we determined that an average of 80% of the embryos which survived showed fluorescent signal, confirming a successful micro-injection (see Fig. 4E).

Using the protocols we developed to micro-inject and culture *P. canaliculata* embryos, we next asked if they could translate exogenous mRNA. After injecting the embryos with mRNA for either GFP or membrane targeted tdTomato, we observed fluorescence in the correct wavelength and subcellular localization (see Fig. 4F). In both cases the fluorescent signal was detectable up to 4 days post injection (dpi).

Overall, we developed tools and approaches that are crucial for making apple snails amenable for a broad variety of experimental designs. Embryos can be collected at any stage of interest and then cultured *ex ovo*, where it is possible to observe and image them over time. Moreover, we optimized micro-injections in zygotes and demonstrated that exogenous mRNA can be used as strategy for gene over-expression or lineage tracing experiments. Together these represent fundamental steps toward bringing robust approaches for genetic manipulations in apple snails.

P. canaliculata has a *pax6* gene highly expressed during both eye development and eye regeneration

pax6 is a regulatory gene with a fundamental role in brain and eye development. In mouse and *D. melanogaster*, *pax6* expression is required for proper eye formation[25,29]. The *P. canaliculata* genome[18,19] has 5 genes annotated as *pax6-like* (NCBI RefSeq GCF_003073045.1). To determine if these genes contain both domains characteristic of *pax6* (PAX and HOX domains) and are similar to the human and fly proteins, we annotated the domains, predicted the 3D folding and evaluated the amino acid conservation for all the sequences.

We found that two out of the five genes identified in apple snails have both PAX and HOX domains, but only one (LOC112559942) has a complete PAX domain and a much higher amino acid conservation than the others (see Fig. 5A and Supplementary Fig. 6A, B and Supplementary Data 4). This result was confirmed by running a phylogenetic relationship and analyzing their expression levels. The gene LOC112559942 is phylogenetically closer to human and fly *pax6* and is more highly expressed in the adult retina than the other candidate genes (see Supplementary Fig. 6C, D). This suggests that LOC112559942 is an ortholog of the human and fly *pax6*.

To gain a better understanding of *pax6* expression and dynamics, we evaluated its expression through RNA-Seq analysis across multiple adult tissues, and during eye regeneration time course and HCR in situ hybridization during embryonic development and eye regeneration. Transcriptomic analysis shows that the retina is the adult tissue where *pax6* is more highly expressed and during complete eye regeneration *pax6* expression increases from 1 to 6 dpa (see Supplementary Fig. 6E, F). Since *P. canaliculata* is characterized by direct development (i.e., lack of metamorphosis or free-living larval stage) we performed HCR on developing embryos and mapped *pax6* expression to the embryonic equivalent of adult organs. HCR during embryo development shows that at 3 days post fertilization (dpf) *pax6* is expressed in the anterior part of the embryos including the cephalic area and the foot. At 5 dpf fluorescent signal can be observed in the eye buds, anteriorly to the eye buds and in the foot. The *pax6* expression seems more clearly confined in the eye stalk at 7 and 9 dpf, when the embryonic development is completed and the embryos are ready to hatch. At these stages, we can also see the expression of *rhodopsin*, a marker for photoreceptor cells, that are differentiating in the embryonic retina (see Fig. 5B). In 9 dpf embryos, at the end of the embryonic development, we also observed the *pax6* expression in the cerebral ganglia together with the neuronal marker, *nec2* (see Fig. 5C). We also performed HCR on adult eye regeneration to validate the transcriptomic analysis. We observed a few isolated *pax6* positive cells in the remaining eye stalk at 1 dpa. At 3, 6 and 9 dpa, *pax6* positive cells were more abundant in the blastema, around and in the optic cup (see Fig. 5D and Supplementary Fig. 6G). At 12 dpa the *pax6* expression is more localized in the regenerating retina where also *rhodopsin* starts being expressed. At 15 and 21 dpa there are cells that are only *pax6* positive, cells that are only *rhodopsin* positive and cells that express both genes (see Fig. 5D, E and Supplementary Fig. 6G). Finally, *pax6* signal is overall reduced at 28 dpa, where we observed *pax6* expression only in the anterior part of the regenerating retina, and posteriorly cells are *rhodopsin* positive and *pax6* negative.

In summary, we found a *pax6* gene in *P. canaliculata* that structurally resembles the human and *D. melanogaster pax6* genes and is expressed in the apple snail eyes, both during development and regeneration.

CRISPR mutant snails reveal *P. canaliculata pax6* is required for eye formation

To test Pax6 function in *P. canaliculata* and evaluate if its role in eye development has been conserved, we applied the CRISPR-Cas9 system in apple snails. Taking advantage of these protocols, we developed for micro-injection and *ex ovo* culture, we established the protocol to generate loss of function mutations through micro-injection of guide-RNA (gRNA) and Cas9 protein (see Supplementary Fig. 7A–C). We targeted three different genes (*pax6*, *dia2* and *pitx*) and we successfully generated mutant lines for all of them (see Fig. 6A–D and Supplementary Fig. 7D–I and Supplementary Data 5). The gene *pax6* was selected because of its known crucial role in vertebrate eye development[29,30], while *dia2* and *pitx*, genes potentially involved in determining the shell chirality[31–34], were targeted to ensure reproducibility and robustness of our protocol for gene knock-out in apple snails.

For *pax6*, a gRNA was designed to target Exon 3 out of the 11 exons present in the gene. F0 individuals were grown to adults and crossed

https://doi.org/10.1038/s41467-025-61681-6

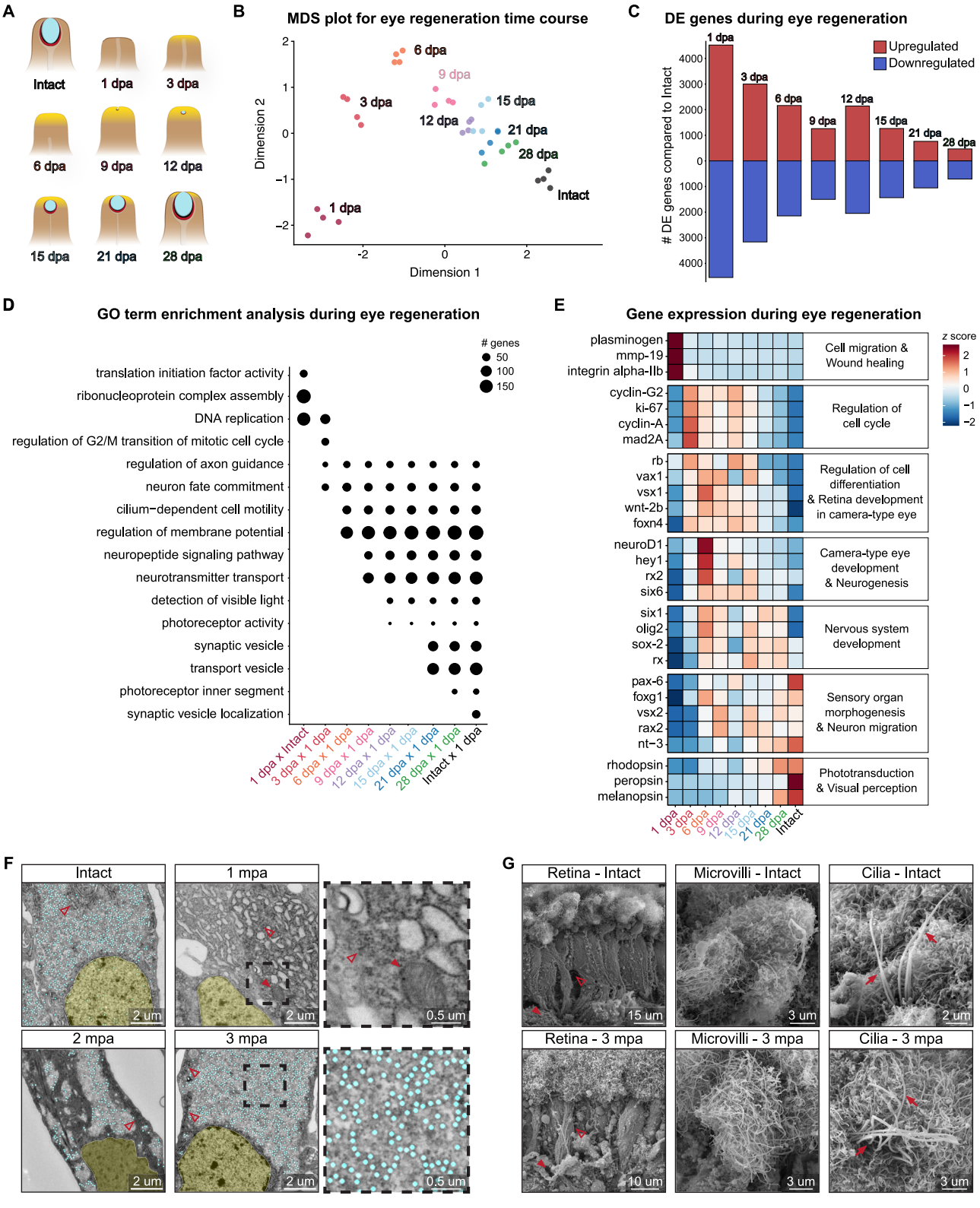

with each other or wild-type animals (see Fig. 6A and Supplementary Fig. 7D–F). The F1s were then genotyped to test for germline transmission of the mutation in the targeted site (see Fig. 6A and Supplementary Fig. 7G) and the animals heterozygous for the mutation were incrossed to generate F2s or outcrossed to maintain the line. Genotypes of F2 siblings confirmed that the mutation was distributed among the offspring following Mendelian inheritance (see Fig. 6A and Supplementary Fig. 7H, I).

The F2 embryos obtained from the *pax6* mutant line were then used to analyze the phenotype. Homozygous mutant embryos at 9 dpf do not have retina nor eye stalk. Close to the tentacle, there is no resemblance of any eye structure, while all the other cephalic organs do not present any observable phenotype (see Fig. 6B). The phenotype was observed in about 25% of the F2 embryos and subsequent genotype of these animals showed that only homozygous mutant embryos presented the phenotype (see Fig. 6C, D). Staining with phalloidin

Fig. 3 | *P. canaliculata* regenerating eyes express genes driving vertebrate eye development. A Schematic representation of the main morphologically defined time points during eye regeneration. Blastema/cell proliferation (yellow), lens (cyan), retina (red). **B** MDS plot of RNA-Seq samples collected during eye regeneration time course. Dimension 1 explains 41.8% of variance and Dimension 2 13.72%. $n = 4$ samples/time point (5 animals/sample) (see Supplementary Fig. 3A). **C** Number of differentially expressed (DE) genes (up-regulated in red and down-regulated in blue) compared to Intact samples [Log Fold Change (LogFC ≥ 0 and FDR ≤ 1e−5]. **D** GO enrichment analysis using significantly up-regulated genes (LogFC ≥ 0 and FDR ≤ 1e−5) in 1 dpa vs Intact and in 3, 6, 9, 12, 15, 21 and 28 dpa vs 1 dpa comparisons to highlight the features recovered throughout regeneration. GO terms used in this representation were manually selected from GO enrichment analysis run on the up-regulated genes obtained from comparing each time point with the previous one (p value ≤ 0.01, q value ≤ 0.05) (see Supplementary Fig. 4 and Supplementary Data 3B, C). **E** Heatmap of gene expression changes during eye regeneration time course. These genes represent the main stages of eye regeneration, and many of them are known, from previous studies, to be involved in vertebrate eye development (z scores calculated from TPMs). Gene categories on the right of the heatmap are based on GO annotations. **F** TEM images of the photoreceptor cytoplasm in the retina of Intact, 1, 2 and 3 months post amputation (mpa) eyes. Nuclei (yellow), photic vesicles (cyan), ribosomes and rough endoplasmic reticulum (empty arrowhead) and mitochondria (full arrowhead). The images are representative of data collected through three independent experiments. **G** SEM images of the retina, photoreceptor microvilli and apical cilia observed in Intact and 3 mpa eyes. At both time points, the retina is constituted by long photoreceptors (empty arrowhead), neuropile (on the bottom, full arrowhead) and microvilli (on the top). The photoreceptor microvilli at 3 mpa show an apical flat and wide expansion of the membrane like the Intact eyes. Cilia (full arrow) have been observed intercalated in the photoreceptor microvilli both in Intact and 3 mpa retina. The images are representative of data collected through three independent experiments.

during an embryonic development time course highlighted that in absence of *pax6* there is no sign of eye formation at any moment of embryogenesis (see Fig. 6E). The earliest time point where eye formation is detected in wild-type embryos is 4 dpf as an area of higher condensation of cell membrane in the cephalic region forms close to the tentacle buds. Mutant embryos at 4 dpf or later do not show the same cellular dynamics and the epithelial cells close to the tentacle buds are homogenously distributed (see Fig. 6E).

Additionally, a behavioral phenotype was observed in *pax6* mutants. Wild-type and heterozygous snails, from the time they hatch, are significantly active and can easily flip on to their foot to move around and explore their environment. Both while on their dorsal side and while moving on their foot, they spread their cephalic tentacles and move them around. Homozygous mutant embryos, on the other side, need to be manually hatched and continuously lay on their dorsal side at the bottom of the tank, are unable to rotate on their ventral side to move using their foot and keep their cephalic tentacles constantly curled close to the head. These animals are unable to independently find food and their long-term survival rate is extremely low although being maintained in sugar-enriched water and hand-fed. Wild-type adult snails whose eyes were amputated did not phenocopy the homozygous mutant behavior and the way they move around and use their tentacles was indistinguishable from the wild types (see Fig. 6F and Supplementary Movie 1). This suggests that the lack of eyes is not the cause of the observed behavioral phenotype, implying that *pax6* is necessary, not only for eye formation, but also for proper development of components that are crucial for locomotion, for the use of cephalic tentacles and foot and maybe, even for gravity perception.

This is the first time that a *pax6* stable knock-out line has been developed in a lophotrochozoan confirming, through loss of function, the conserved role of this transcription factor in eye development. We showed that at least one copy of *pax6* is necessary to activate the eye development program and that *pax6* role during brain development might be conserved in apple snails. Overall, the data presented here show that *P. canaliculata* is now a genetically tractable research organism that can be adopted to study gene function in biological processes of interest.

Discussion

Our eyes are complex and delicate organs that can only rarely recover from damage or aging. Among research organisms, some vertebrates, like zebrafish, salamanders and frogs, can recover from minor injuries to specific retinal cell types or individual eye components[7,35]. Meanwhile, some invertebrates, like planarians, can fully regenerate their eyes, but their visual system has a very different and more simple anatomical structure[6]. Our work aimed to bridge this gap by identifying an organism capable of regenerating camera-type eyes, which although classically associated with vertebrates, can also be found in some invertebrates[3–5]. Here, we report the discovery that the camera-type eyes of the freshwater apple snail *P. canaliculata* can fully regenerate. We also developed protocols and tools to demonstrate the amenability of this novel regeneration organism to genetic manipulation. These resources not only open the door to answering fundamental questions about camera-type eye regeneration but also make *P. canaliculata* an innovative system where numerous other aspects of biology can be explored, since this is one of the very few mollusks where stable mutant lines have been established[36].

Animal visual systems: anatomical similarities and differences

The visual system is important for many aspects of animal physiology, such as navigating the environment, mating and regulating activities throughout the day. The eyes are one of the main components of the visual system and they can be classified based on their anatomical structure, components and light path[3–5]. While vertebrates have camera-type eyes, invertebrates show a broader spectrum of eye types[3–5]. The taxon *Mollusca* is particularly interesting since they have representation of all the main 7 types of eyes described so far, including pigmented cups and camera-type eyes[3–5,24]. Gaining further understanding on the anatomy, cell biology and gene expression of additional molluscan eyes will represent a step towards a better understanding of eye evolutionary history. This will provide evidence on which elements have been shaped by either parallel or convergent evolution among mollusks or between mollusks and other taxa.

Here, we show that the gastropod *P. canaliculata* has camera-type eyes. Interestingly, the animal environment and behavior are correlated to specific properties of some eye components, such as cornea and lens[3–5]. The human lens is biconvex, aquatic animals, such as zebrafish, have a spherical lens, and nocturnal animals, like mice, usually have larger lenses[3–5]. Apple snails are aquatic and relatively active during the night and their lenses are round and large, key features usually associated to these traits.

Vertebrates have an inverted retina, with the apical part or outer segment of the photoreceptor pointing towards the external part of the eye[5]. These photoreceptors (rods and cones in humans) are defined as ciliary because of a modified cilium present between the inner segment, more basal with the nuclei and other organelles, and the outer segment, constituted by membrane discs and folds to host the visual pigments, such as opsins[21,37]. Like cephalopods and other invertebrates with camera-type eyes[5,38], *P. canaliculata* retina is not inverted and thus the outer segment of the photoreceptor points towards the lens. The pigmented layer in the retina contains dark pigments that creates a physical barrier to protect deeper tissue from the light and provide directional information about the light source[3–5]. Interestingly, the pigmented layers of both vertebrates and *P. canaliculata*, although differently positioned relative to the retina, are

https://doi.org/10.1038/s41467-025-61681-6

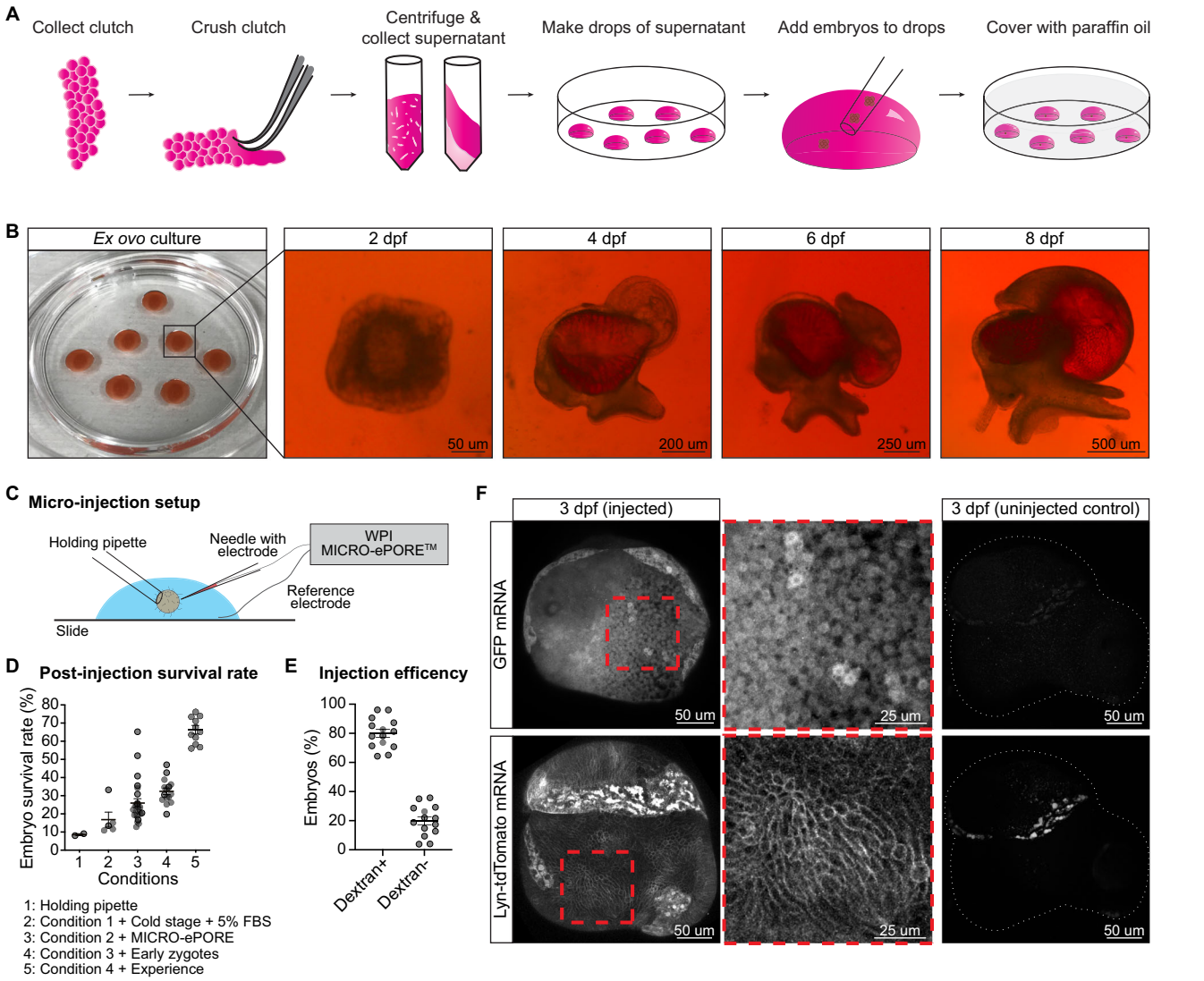

Fig. 4 | *P. canaliculata* zygotes can be collected, micro-injected with exogenous mRNA and cultured *ex ovo*. **A** Schematic representation of *ex ovo* culture protocol steps. Clutches are collected, crushed and centrifuged. The supernatant is collected and used to make drops where the embryos can be cultured. Everything is covered with paraffin oil to avoid evaporation. **B** Images of embryos cultured at 0 days post fertilization (dpf) and developing *ex ovo*. The images are representative of data collected through 6 independent experiments with more than 10 embryos in each experiment. **C** Schematic representation of the setup used for *P. canaliculata* zygote micro-injection (see Supplementary Fig. 5B, C). **D** Embryonic survival rate after micro-injection using different micro-injection protocols. Each dot represents an injection session with 50–100 embryos. **E** Percentage of embryos Dextran-positive, used as read-out of successfully injected embryos. Each dot represents an injection session with 50–100 embryos. **F** Confocal images of 3 dpf embryos injected with GFP mRNA or Lyn-tdTomato mRNA. GFP localizes in the cytoplasm, the membrane targeted tdTomato localizes in the cell membranes and the uninjected controls show some autofluorescence with a stereotypical localization in the red channel. Data are represented as mean ± SEM. The images are representative of data collected through two independent rounds of injections with more than 20 embryos each.

localized immediately behind the outer segment of the photoreceptor, highlighting conserved function.

The photoreceptor anatomy, their visual pigments and their signal transduction pathways have a significant role in determining what the animals can see and consequently are strongly correlated with animal behaviors. Most photoreceptors found in invertebrates, independently from the eye type, are rhabdomeric photoreceptors. These photoreceptors do not have a modified cilium and their outer segment is constituted by microvilli instead of stacked membranes[21,37]. Here, we show that *P. canaliculata* has rhabdomeric photoreceptors. However, we also observed cells with centrioles and/or cilia and detected the expression of rod and cone-specific genes. Although additional data needs to be collected in apple snails, recent examples of invertebrates with both ciliary and rhabdomeric photoreceptors have been reported[21].

As previously observed for other mollusks, *P. canaliculata* eyes merge together anatomical, cellular and molecular features that historically were considered exclusive for vertebrate or insect eyes. This highlights the need to study the visual system of more species at all levels of organ complexity to populate the phylogenetic trees with data that will clarify the evolutionary history of this organ.

Regeneration of missing body parts and specifically eyes

Regeneration is the process of replacing damaged or lost body parts. Regeneration can happen through different mechanisms; the more studied mechanisms are morphallaxis (reorganization of pre-existing tissue) and epimorphosis (intense cell proliferation and blastema formation)[1,2,39]. The regeneration of sensory organs, such as the eyes, represents a unique paradigm to study, considering their important function and their complex anatomy. Eyes are composed of multiple

https://doi.org/10.1038/s41467-025-61681-6

structures perfectly tuned with each other, with relevant neuronal components that are precisely wired to the brain for information integration and interpretation[40]. Though salamanders can regenerate the lens and both zebrafish and salamanders can regenerate retina cell types, there are no known examples of adult vertebrates that can fully regenerate their eyes after complete resection[7,10]. Although the regeneration of these visual system components in vertebrates happens without the formation of a blastema, processes such as cell

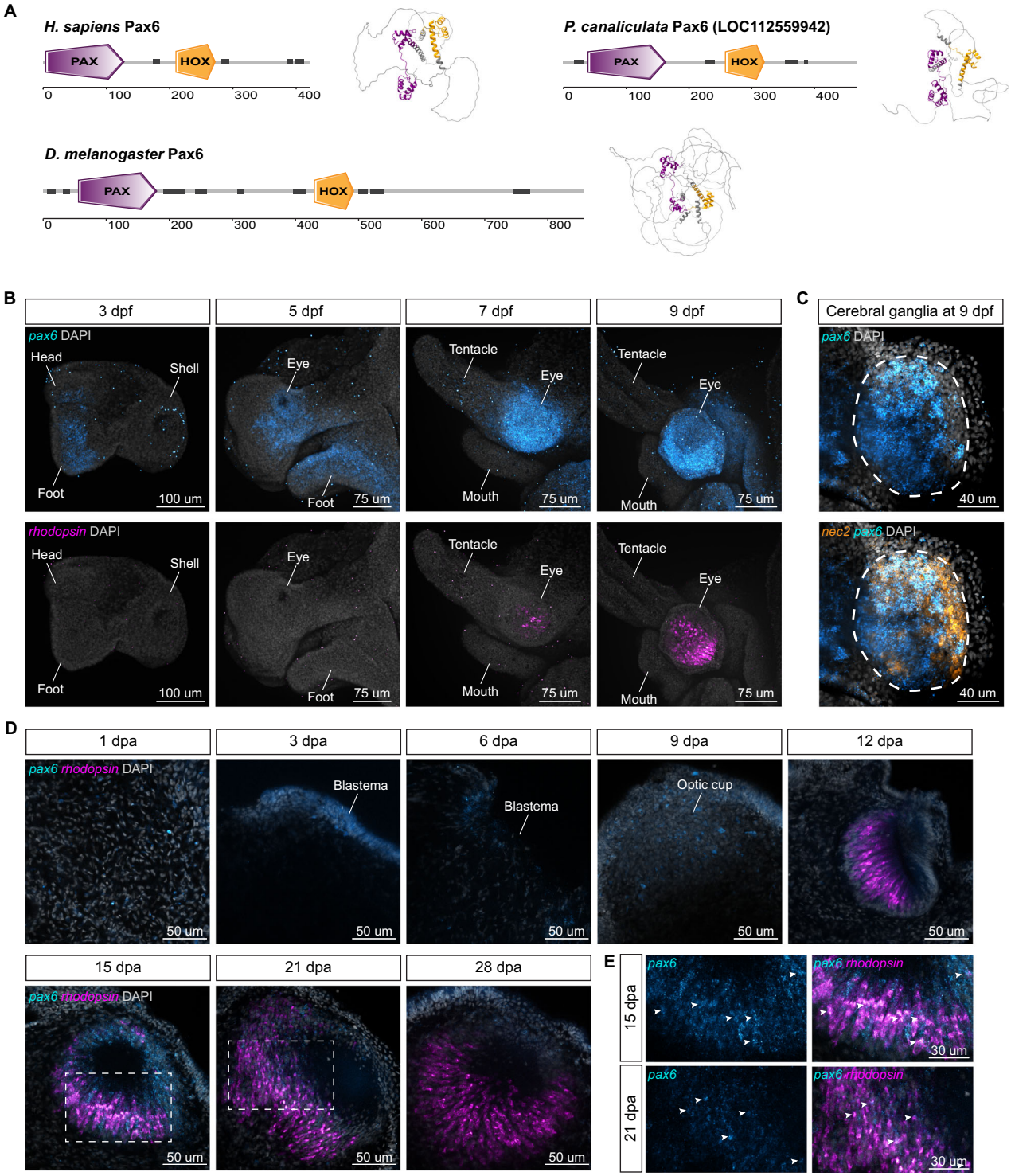

Fig. 5 | *P. canaliculata* has a *pax6* gene highly expressed in the eye buds. **A** Domain and 3D-folding predictions for human, *D. melanogaster* and *P. canaliculata* *pax6* genes. Purple = PAX domain, orange = HOX domain, dark gray = disordered regions (see Supplementary Fig. 6). **B** Confocal images of *pax6* (cyan) and *rhodopsin* (magenta) HCR during embryonic development. *rhodopsin* highlights the localization of the retina and the differentiation of the photoreceptors. The images are representative of five embryos. **C** Confocal images of *pax6* (cyan) and *nec2* (orange) HCR during embryonic development. *nec2*, also known as *proprotein convertase 2* (*pc2*) or *prohormone convertase 2*, has been used as marker for the nervous system. The images are representative of five embryos. **D** Confocal images of *pax6* (cyan) and *rhodopsin* (magenta) HCR on eye stalk whole mount during adult eye regeneration. The images are representative of five samples. **E** Detail of the 15 and 21 dpa regenerating retina. White arrowheads highlight cells expressing both *pax6* (cyan) and *rhodopsin* (magenta). The images are representative of five esamples.

https://doi.org/10.1038/s41467-025-61681-6

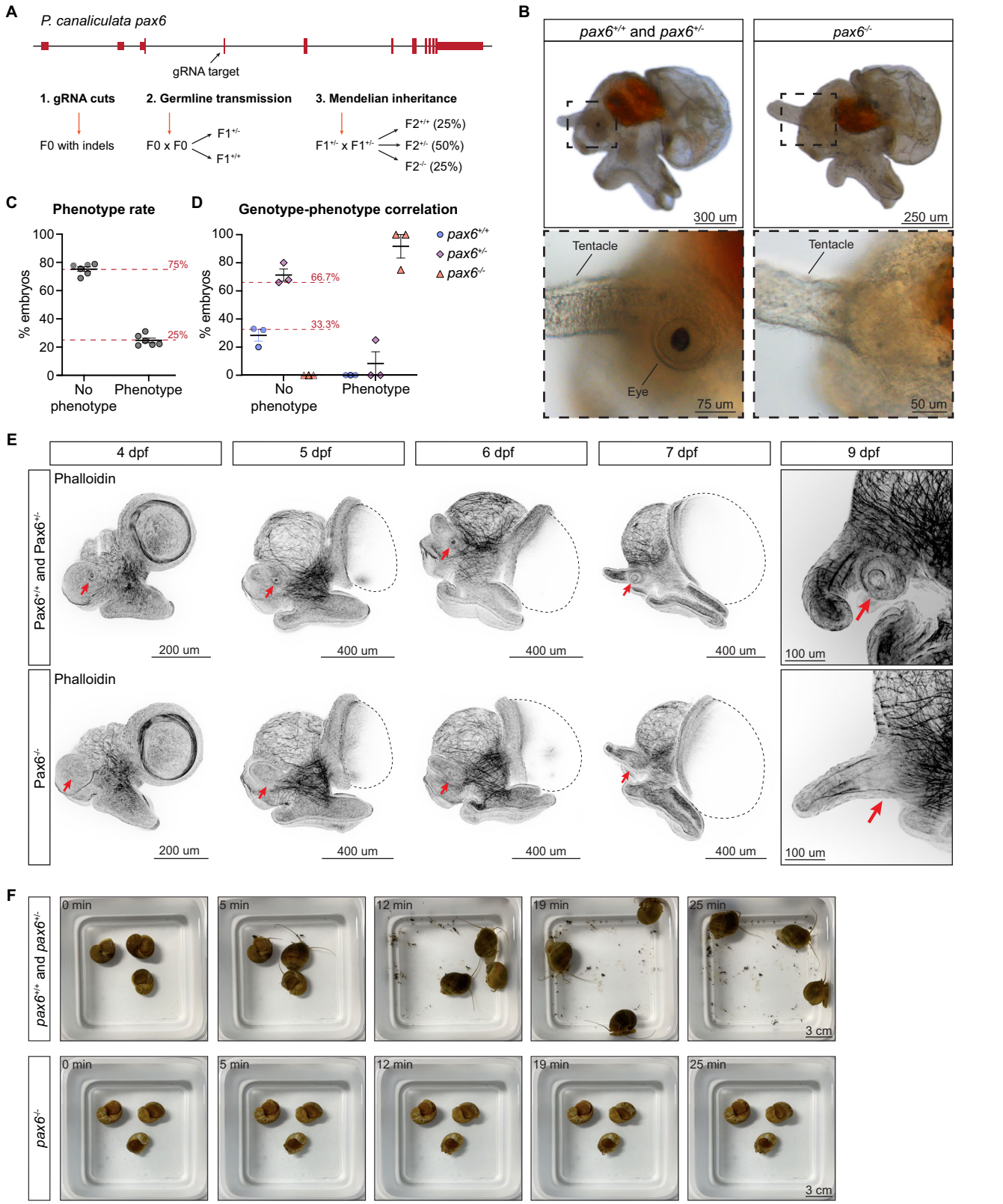

proliferation and cell differentiation can be observed. Adult newts lens regeneration is a clear example of transdifferentiation, where the iris pigment epithelial cells give rise to lens cells[9]. Zebrafish regenerate retinal cells through Müller glial cell activation, dedifferentiation, proliferation and differentiation, while adult salamanders regenerate cells in the neural retina by reprogramming retinal pigmented cells[7,10].

Lophotrochozoans, and specifically gastropods, are known for their regeneration potential, with some more extreme cases of entire eye or even entire head regeneration[11–14,41,42]. Here, we show that adult and sexually mature *P. canaliculata*, with very limited active growth and neurogenesis during homeostasis, can regenerate their camera-type eyes after full amputation. This is a remarkable characteristic, since other organisms, like the snail *Achantina fulica*, lose or

Fig. 6 | CRISPR mutant snails reveal *P. canaliculata pax6* is required for eye formation. A Schematic representation of the *P. canaliculata pax6* genomic region, the gRNA target site, and the crossing strategy used to establish a stable mutant line and to obtain homozygous mutant animals (see Supplementary Fig. 7 and Supplementary Data 5). **B** Images of wild-type and *pax6*$^{-/-}$ 9 dpf embryos and insets of the region at the base of the cephalic tentacle. Wild-type and *pax6*$^{+/-}$ animals have eyes while the *pax6*$^{-/-}$ snails lack all the eye bulb and eye stalk components. **C** The percentage of F2 embryos with the "lack of eye" phenotype corresponds to the expected 25%. $n = 6$ clutches. **D** Correlation between genotypes and phenotypes in F2 embryos shows that the lack of eyes corresponds to homozygous mutants. $n = 3$ clutches. **E** Confocal images of wild-type and *pax6*$^{-/-}$ embryos stained with phalloidin during a developmental time course. Phalloidin shows that at 4 dpf there is a first morphological evidence of eye formation through cell wall contraction in the cephalic area of the embryos. The red arrows point at the area where the eye develops (in wild-type and *pax6*$^{+/-}$ snails) or where it should be developing (in *pax6*$^{-/-}$ snails). **F** Still images of time lapses showing adult wild-type and *pax6*$^{-/-}$ snails free to move in their tanks (see Supplementary Movie 1). Data are represented as mean ± SEM.

significantly decrease their regeneration abilities with age[14]. *P. canaliculata* eye regeneration happens through epimorphosis, with intense cell proliferation and formation of a blastema. The cellular and molecular mechanisms used for this regeneration remain unknown. In several invertebrates with high regenerative potential, stem cell populations with the potential of being activated after injury have been identified[2,39,43,44]. We speculate that apple snails also have a stem cell population responsible for the formation of the blastema, although additional experiments are required. Additionally, the potential contribution of cell dedifferentiation or transdifferentiation, similar to what has been observed in vertebrates, cannot be excluded.

Finally, previous evidence underlines the importance of both the immune system and the nervous system in creating regeneration permissive niches and supporting the new tissue growth. Microglia cells have been shown to be necessary for retinal cells regeneration in zebrafish[9,45]. In apple snails, it has been previously observed that clodronate treatment depletes circulating phagocytic hemocytes and delays the formation of the blastema after the amputation of the cephalic tentacle[46]. This suggests that the roles of the immune and nervous systems in *P. canaliculata* eye regeneration need to be further investigated.

Altogether, *P. canaliculata* is an extraordinary organism that brings together the presence of camera-type eyes and a high regenerative potential in adults. This represents a unique opportunity to study aspects of complex sensory organ regeneration.

Established and emerging organisms in research

Currently established research organisms have been selected in the past for practical reasons such as ease to maintain in captivity and year-round and frequent breeding that produces a considerable number of offspring. These animals also have a relatively fast generation time and some particularly interesting or unique features that made them essential to advance specific fields (e.g., transparent zebrafish embryos or low chromosome number in *D. melanogaster*)[47,48]. Because of their genetics and widespread use, these were among the first animals in which methods to test gene function were developed and whose genomes were sequenced[49,50]. Recently, technological advances such as the reduced cost of sequencing and the advent of CRISPR systems have allowed the establishment of new research organisms[51–58].

The freshwater apple snail *P. canaliculata* is a resilient animal that can complete its life cycle in an aquarium and breed year-round providing hundreds of embryos per clutch[16]. Apple snails are diploid[17] and their genome is non-duplicated and smaller than many other mollusks[36,59], which facilitated its sequencing[18,19]. These are important features for establishing *P. canaliculata* as a genetically tractable organism. Here, we showed how we overcame challenges related to collecting and micro-injecting zygotes, raising F0s to adults and genotyping animals to establish the first stable mutant lines of apple snails using the CRISPR-Cas9 technology. Moreover, multiple mutant lines were established to confirm that this was a robust and reproducible protocol. In this study, F2 individuals were needed to assess the phenotype but the injection of a higher concentration of RNP, like it has been shown in *Capitella teleta*, *Crassostrea gigas* and *Doryteuthis pealeii*, could reduce mosaicism allowing for phenotype determination in F0 crispants[55,60,61]. It is important to note that the different concentrations of gRNA and Cas9 proteins were tested before the increased survival rate obtained through the use of the MICRO-ePORE, early-stage embryos and increased expertise.

P. canaliculata has many features that make it a system with potential to be extensively used in the laboratory and it also has the remarkable and rare feature of being able to fully regenerate camera-type eyes, making it a system of great value to uncover the mechanisms of complex sensory system development and regeneration. This work provides fundamental tools which open avenues for the scientific inquiry of molluscan and lophotrochozoan biology.

Shared regulatory network for eye development

In the past few decades, many studies were performed to gain a better understanding of the GRNs controlling eye morphogenesis and specific cell type differentiation[28,62]. The transcription factor *pax6* has been reported in multiple species, with and without camera-type eyes, as one of the initiators of eye development. Studies in *Drosophila* demonstrated that *pax6* expression is both necessary and sufficient for eye development[63]. In vertebrates, optic vesicles and optic cup determination happens through a signaling cascade activated by Pax6 and involving several other eye field transcription factors[28,64]. Once the eye field has been determined and organized into specific regions, the neural retina progenitors start expressing genes downstream of *pax6* that specify the retinal cell types[28]. *P. canaliculata* has most of these genes in its genome and many are expressed in the adult eye bulb. This provides an opportunity to compare and contrast differences in the GRNs for eye development in between *P. canaliculata* and other models. For example, *P. canaliculata* Pax6 has well conserved sequence, domains and 3D structure when compared to human PAX6 and it is expressed in both adults and embryonic eye. Pax6 is known to be involved not only in development of the eyes but also of the brain, nose, pancreas and pituitary gland[29,65]. Previous work on lophotrochozoans showed the presence of a *pax6* gene and its expression related to eye and brain development[6,66,67]. Here, we knocked-out *pax6* for the first time in a lophotrochozoan, showing that *pax6* is necessary for eye development, it likely plays a role in the development of cerebral ganglia and its absence is lethal, similar to what has been observed in mice[30]. This suggests a conserved function for *pax6* between vertebrates and apple snails. We can extend this type of analysis to other components of the GRN.

So far, we explored the function of *pax6* gene during embryonic development. Based on our transcriptome analysis and HCR results showing *pax6* expression during adult eye regeneration, we hypothesized that this gene also plays a crucial role in adult eye regeneration. Future experiments will test the role of *pax6* in adults, as well as define the GRN to which *pax6* belongs providing exciting information about the mechanisms that control and allow complete regeneration of camera-type eyes in *P. canaliculata*. The experiments we have conducted illustrate how apple snails are an excellent model system poised for utilizing a broad range of experimental approaches to gain mechanistic insights into the evolution, development and regeneration of camera-type eyes.

Methods

Animal husbandry

The *Pomacea canaliculata* colony at the Stowers Institute for Medical Research (Kansas City, USA) was established starting from specimens

shipped from the University of Modena and Reggio Emilia (Modena, Italy) where a colony of apple snails was maintained for more than 6 years. The apple snails were maintained at 25–27 °C on a light-dark cycle of 14 and 10 h, respectively. They were fed three times a week with a variety of green leaves and kale or calcium enriched pellets to support shell growth. System water was the result of deionized water (diH_2O) mixed with a variety of salts (2.15 uM $CaCl_2$, 0.95 uM $MgSO_4$, 1.88 uM $NaHCO_3$ and 0.02% *P*-Remineraliz™ (Brightwell® Aquatics, USA)) to reach pH = 7.5, osmolarity = 1100 uS, alkalinity 69 ppm, carbonate hardness 248 ppm, 71.53 mg/l Calcium, 21.97 mg/l Magnesium, 2.07 mg/l Potassium, 87.32 mg/l Sodium, 77.36 mg/l Sulfate and additional elements in lower concentrations. pH was maintained constant through a Sodium Bicarbonate automatic dosing system. Additionally, daily water changes (10–30% of total water volume) and debris siphoning helped maintaining good water quality. The snails were maintained following the guidelines from the IACUC veterinary and the requirements specified in the USDA/APHIS permits #P526P-16-03927, #P526P-19-04241, #P526P-22-07053, #526-23-222-08147 and # 526-24-304-32436.

Adult dissection

Unless differently specified, we used adult apple snails with shell length (Antero-Posterior axis) ≥ 27 mm and from 3 to 7 months old. To access their cephalic area, the apple snails were anesthetized through a 10 min incubation in ice and then the operculum was gently pulled with self-clamping forceps. Surgical micro-scissors and tweezers were used to fully remove the eyes, to collect intact or regenerating tissue or to isolate the lens or the retina. Images were acquired with a Zeiss Stemi SV 11 Apo stereomicroscope equipped with a Lumen*era* Infinity3 camera or with a Leica M205 FA stereomicroscope equipped with a Leica DFC310 FX camera. After image acquisition, Fiji software[68] was used for exporting and processing images.

Embryo collection

To collect embryos in the first 24 h post fertilization (hpf), clutches were incubated in 15 mg/ml L-cystein pH 7.5 for 3 min. Then, they were moved in Petri dishes while the L-cystein solution was diluted 1:1 with Embryo Media (6 mM KCl, 6.7 mM $CaCl_2$, 3.3 $MgCl_2$, 1.7 mM HEPES, 33.62 mM NaCl in diH_2O). We individually opened all the capsules with tweezers and then alternated gentle swirls of the mix with embryo harvesting using a stereomicroscope. The gentle swirls helped the embryos to be released from the perivitelline fluid (PVF). To collect embryos after 24 hpf, the capsules were crushed in Embryo Media with tweezers in dishes. Gentle swirls of the media helped to release the embryos from the PVF. Embryos sink on the bottom of the dish at all stages. Since embryos younger than 4 dpf stick to plastic and glass, 5% FBS was added to Embryo Media.

Hematoxylin & Eosin (H&E) morphological staining

Immediately after collection, the samples were fixed in 4% paraformaldehyde (PFA) at 4 °C overnight (ON) on a rotator. After fixation, the samples were incubated twice in 1x PBS with 0.5% Triton X-100 (PBSTx 0.5%) for 20 min, in 50% MeOH in diH_2O for 10 min and in 100% MeOH for 10 min. Finally, the samples were stored in clean 100% MeOH at −20 °C.

To embed the samples in paraffin, we processed them using a Milestone PATHOS Delta Microwave Tissue Processor. The incubations we performed were: 70% EtOH for 4 min, 100% EtOH for 10 min at 65 °C, 100% isopropyl alcohol for 45 min at 68 °C, Paraffin Type 9 (Epredia #8337) at 70 °C for 10, 10, 2, 2 and 2 min, and finally in Paraffin Type 9 at 65 °C for 27.5 min. The samples were stored at room temperature (RT) in cassettes until they were ready to be oriented and embedded in paraffin using a LEICA EG1150H Embedding Center. The samples were sectioned at a 7–8 um thickness onto charged glass slides (Fisher Scientific #22-042-924) using an Automated Rotary Microtome (HistoCore AUTOCUT #149AUTO00C1 and #14051956472) and an Illuminated Tissue Bath set at 42 °C (230 V) (Boekel Scientific #145951-2). Slides were dried in a dry oven at 36 °C for at least 4 h and then stored at RT.

Sections were deparaffinized and stained with ST Infinity H&E staining system kit (Leica #3801698) using a Leica ST5010 Autostainer XL. Slides were baked for 10 min at 60 °C, then they were incubated: three times in 100% xylene over 9 min, three times in 100% EtOH over 3 min, in 80% EtOH for 1 min, in diH_2O for 1 min, in Hemalast for 30 s, in Hematoxylin for 2 min, in diH_2O for 2 min, in Differentiator for 45 s, in diH_2O for 1 min, in Bluing for 1 min, in diH_2O for 1 min, in 80% EtOH for 1 min, in Eosin for 30 s, three times in 100% EtOH over 9 min and three times in 100% xylene over 3 min. Finally, the coverslips were mounted with Surgipath Micromount (Leica #3801731) using a Leica CV5030 Fully Automated Glass Coverslipper and dried for 15 min at RT.

Images were acquired with a Leica DM6000 B upright microscope equipped with a Leica DFC425 camera or with an Olympus SlideScanner VS140 and a 40x objective. After image acquisition, Fiji software[68] was used for exporting and processing images and measuring the eye components.

Immunohistochemistry (H3P/BrdU)

Snails were anesthetized and eyes were fully removed as already mentioned. Snails were anesthetized again 24 h before collecting the regenerating tissue and injected on the left side of the body with 3 mg of BrdU (Sigma #B5002) diluted in 500 ul of diH_2O. The regenerating tissue was collected 24 h post injection (hpi) and fixed, washed, dehydrated, embedded in paraffin and sectioned as already mentioned.

Sections were deparaffinized using a Leica ST5010 Autostainer XL by baking the slides for 10 min at 60 °C and by incubating them: three times in 100% xylene over 9 min, three times in 100% EtOH over 3 min, in 80% EtOH for 1 min and in diH_2O for 1 min. Sections were bleached for 1 h and 30 min under direct light in 5% formamide, 1% H_2O_2 and 0.5x SSC (1x SSC is 150 mM sodium chloride and 15 mM sodium citrate, pH 7.0 with citric acid) in diH_2O. After rinsing 3 times in diH_2O, we performed heat-induced antigen retrieval through an incubation in citrate buffer (0.1 M citric acid and 0.1 M trisodium citrate in diH_2O, pH 6.0) at 95 °C for 15 min in a BioGenex EZ-Retriever® IR – Antigen Retrieval System. Slides were allowed to cool down for 20 min and then they were incubated in 1x PBS with 0.1% Tween 20 (PBSTw 0.1%) for 30 min. Blocking of nonspecific antibody binding was performed using Background Buster (Innovex #NB306) for 45 min at RT. Slides were washed three times with PBSTw 0.1% over 15 min and then incubated with 1:300 Rabbit anti-H3P (Millipore #05817 R clone 63-1C-8) and 1:300 Mouse anti-BrdU (BD Biosciences #347580 clone B44) for 1 h at RT. Slides were washed three times with PBSTw 0.1% over 15 min and then incubated with 1:300 Alexa488 Donkey anti-Rabbit (Biotium #20015), 1:300 Alexa568 Donkey anti-Mouse (Biotium #20105) and 1:500 DAPI (Biolegend #422801) in Background Buster for 90 min at RT. Slides were washed three times with PBSTw 0.1% over 15 min and then the coverslip was mounted using Prolong Gold mounting media (Thermo Fisher Scientific #P36984).

Images were acquired with a Zeiss LSM 700 confocal and processed with Fiji software[68] while the number of positive cells were calculated manually drawing an ROI around the regenerating tissue/blastema and using custom plugins and macros in Fiji similar to the procedure in previous reports[69].

Electron microscopy - TEM processing

Immediately after collection, samples were fixed in EM fixative (2% glutaraldehyde and 2.5% paraformaldehyde in 50 mM sodium cacodylate buffer, with 1 mM calcium chloride and 1% sucrose, pH 7.35) for 1 h at RT on a rotator. After fixation, the samples were stored in EM fixative at 4 °C.

All the following steps were completed at 4 °C unless otherwise noted and all rinsing steps were 15 min each. Samples were rinsed 3 times with 50 mM sodium cacodylate buffer followed by secondary fixation with buffered 1% osmium tetroxide for 1–2 h at RT. Three more rinses with 50 mM sodium cacodylate buffer and three with water were carried out before *en bloc* staining with 0.5% aqueous uranyl acetate at 4 °C ON. After rinsing three times with water again, samples were dehydrated in a graded series of acetone (25%, 50%, 75%, 90% and 100%) for 10 min each. Cold 100% acetone was used for an additional incubation and moved to RT for 10 min, followed by a final 100% acetone incubation at RT for 10 min. Resin infiltration was carried out at RT with a graded series (1:2, 1:1, 2:1) of SPURR low viscosity resin (EMS #1430 hard formulation) with acetone for 30 min to ON each step depending on sample size, followed by 4 pure resin incubations over 2 days. Samples were embedded in SPURR resin in flat molds (Ted Pella #105) and cured at 60 °C for 48 h.

Once cured, sections were cut between 60 nm and 100 nm with a Leica UC6 or UC7 ultramicrotome and Diatome ultra 45 diamond knife and placed on Formvar®/Carbon coated slot grids or on glass slides. Sections were then post-stained at RT with Sato's triple lead stain for 3 min, 4% uranyl acetate in 70% MeOH for 4 min and Sato's triple lead stain again for 5 min. Grids were imaged in a Tencnai BioTwin TEM at 80 kV with a Gatan UltraScan 1000 CCD camera, or a Zeiss Merlin SEM using aSTEM4 detector at 30 kV and 141 pA with either SmartSEM (Zeiss) or Atlas 5 (Fibics, inc.) acquisition software. Slides were coated with 4 nm of carbon in a Leica ACE600 and imaged in a Zeiss Merlin SEM with a 4 quadrant BSD detector at 8 kV and 700 pA using Atlas 5 acquisition software.

For vesicle analysis, sections were cut at 60 nm on slides and sections post-stained and coated with carbon as already mentioned. For each eye an overview of one section at 100 nm pixel size and 2 areas of interest at 6 nm pixel size was acquired on a Zeiss Merlin SEM as stated above using Atlas 5 software.

Acquired images were exported and processed using Fiji software[68]. Photic vesicles were identified using the deep learning package DeepFiji[70] after hand annotating examples.

Electron microscopy - SEM processing

Immediately after collection, the samples were fixed and stored as already mentioned.

All the following steps were completed at RT and all rinsing steps comprised 2 quick rinses and then 5 rinses over 25 min. Staining and secondary fixation solutions were all 1% aqueous and filtered with a 0.2 um syringe filter. Samples were post-fixed and stained with tannic acid, osmium tetroxide, thiocarbohydrazide (TCH), and osmium tetroxide sequentially, each for 1 h and rinsed in ultrapure water before each incubation. After rinsing again with ultrapure water, samples were dehydrated in a graded series of EtOH (30%, 50%, 70% and 90%) and 3 pure EtOH incubations for 10 min each. Samples were loaded into a 4 or 12 sample holder (Tousimis #8763 or #8762) for critical point drying in a Tousimis Samdri-795. After drying, samples were mounted on aluminum stubs with carbon stickers, coated with 4 nm gold palladium in a Leica ACE600, and imaged in a Zeiss Merlin SEM at 8 kV and 150 pA with SE detector and a working distance of 8 mm, using SmartSEM or Atlas 5 acquisition software.

Acquired images were exported and processed using Fiji software[68].

Bulk RNA-sequencing (RNA-Seq)

Adult tissues and organs were collected and total RNA from each sample was extracted using Trizol® Reagent (Ambion #15596026) and following the protocol from the producer. The purified RNA quantity and quality was determined by Qubit® 2.0 Fluorometer (Invitrogen) and Agilent 2100 Bioanalyzer (Agilent Technologies), respectively.

mRNA-Seq libraries were generated from high-quality total RNA as assessed using the Bioanalyzer (Agilent) or the LabChip GX (Caliper Life Sciences). Libraries were made according to the manufacturer's directions for the TruSeq Stranded mRNA LT Sample Prep Kit – sets A and B (Illumina #RS-122-2101 and #RS-122-2102) or TruSeq Stranded mRNA Library Prep kit (48 Samples) (Illumina #20020594) or TruSeq RNA Single Indexes Sets A and B (Illumina #20020492 and #20020493). Resulting short fragment libraries were checked for quality and quantity using the Bioanalyzer (Agilent) or the LabChip GX (Caliper Life Sciences) and the Qubit Fluorometer (Life Technologies). Libraries were pooled, re-quantified and sequenced utilizing RTA and instrument software versions current at the time of processing.

In more details, mRNA-Seq libraries for retinas ($n = 3$ samples) were generated from 250 ng of high-quality total RNA and libraries were sequenced as 50 bp single reads on 1 lane of an Illumina HiSeq 2500 flow cell.

mRNA-Seq libraries for cephalic tentacles ($n = 3$ samples) were generated from 150 ng of high-quality total RNA and libraries were sequenced as 100 bp paired reads on 4 Rapid Run flow cells using the Illumina HiSeq 2500 instrument.

Samples of intact eyes and regenerating tissue after full eye bulb amputation ($n = 4$ samples) were collected pooling together tissue from 5 animals/sample. mRNA-Seq libraries for these samples were generated from 100 ng of high-quality total RNA and libraries were sequenced as 50 bp single reads on a P3 flow cell using the Illumina NextSeq 2000 instrument.

mRNA-Seq libraries for all the other samples ($n = 1$ sample) were generated from 200 ng of high-quality total RNA and libraries were sequenced as 100 bp paired reads on 6 Rapid Run flow cells using the Illumina HiSeq 2500 instrument as well as 150 bp paired reads on 2 Illumina MiSeq flow cells.

RNA-Seq analyses

RNA-Seq reads for all experiments were aligned to the REFSEQ genome and gene models for *P. canaliculata* (GCF_003073045.1) using the STAR alignment program (v2.7.3a)[71]. TPMs were calculated using RSEM (v1.3.0)[72].

The relationship between RNA-Seq samples was assessed with MDS and Spearman correlation on normalized counts. MDS plot was generated with all genes and the Spearman correlation plot with the top 1000 genes with highest mean across time points. Differential Expression Analysis (DEA) was performed using the R package edgeR[73–75]. DEA was performed using 1) the intact eye as a reference, 2) the 1 dpa eye as a reference and 3) in a pairwise manner with adjacent timepoints using the earlier time point as the reference for the later one. Differentially expressed genes were defined by setting an FDR cutoff of 1e−5 and a logFC of 0. Additional data manipulation was performed with the tidyverse R package collection[76].

To perform Gene Ontology (GO) Enrichment[77], it was necessary to annotate the REFSEQ genes with GO terms. Terms used were derived by combining GO terms from Interproscan (5.42–78.0) results and OMA (v2.4.2) mappings[78–80]. Annotations were put into an "org" file using the AnnotationForge R library[81].

GO Enrichment analysis was performed with R package clusterProfiler[82,83]. Figures were made using R libraries GOsemsem, cowplot and enrichplot[84–86]. The p value cutoff for term enrichment was 0.05 and a q value of 0.01. GO terms were explored using GO-Figure!'s semantic similarity scatterplots[87] and manually selected for display.

Ortholog analysis

Domain prediction and domain images for genes annotated as *pax6* in *Homo sapiens*, *Drosophila melanogaster* and *P. canaliculata* were created using SMART[88]. Structures for *pax6* genes were generated with ColabFold (v1.5.2)[89,90] and visualized with ChimeraX[91]. Multiple sequence alignment was made with MUSCLE[92,93]. OMA (v2.5.0) was

used to identify ortholog pairs for comparison of *P. canaliculata* genes to *H. sapiens* and *D. melanogaster*[78].

Ex ovo embryo culture

To prepare the perivitelline fluid extract (ePVF) for culturing the embryos *ex ovo*, clutches (1 or 2 dpf) were incubated in 10% bleach for 3 min and then rinsed three times with diH_2O. The clutches were moved on a dry Petri dish, individually crushed with tweezers, moved in a 2 ml tube and centrifuged at 4 °C for 40 min at 21,000 × *g*. The supernatant was moved in a 1.5 ml tube and stored at −20 °C. The PVF extract can be frozen and thawed multiple times. Because of the nutritious nature of the PVF, autoclaved plastics and clean surfaces help to reduce contaminations. Each ePVF aliquot, coming from an individual clutch, was tested for contaminations and for extract quality using wild-type embryos. For this test, clutches (1 or 2 dpf) were incubated in 10% bleach for 3 min and then rinsed three times with diH_2O. Embryos were collected as already mentioned and then washed three times in 5% FBS in Embryo Media. It is important to keep clutches separate and process them individually.

To set up an embryo culture, the lid of a 30-mm Petri dish was placed facing up inside a 60-mm Petri dish. Drops of ePVF extract were placed inside the 30-mm Petri dish lid and 3-4 embryos were pipetted inside the ePVF extract drop. If the drops are too small or if too much Embryo Media is released in the drops together with the embryos, the culture might not work. Finally, the lid was filled with about 3.0–3.5 ml of paraffin oil (MilliporeSigma #PX0047-1) to cover all the drops. The *ex ovo* cultures were stored inside 60-mm Petri dishes at RT in the dark and they were checked regularly for contamination, embryo growth or formation of bubbles that could cause them to dry out.

Zygote micro-injections

Embryos were harvested as soon as possible as already mentioned and then split into two Petri dishes in 5% FBS in Embryo Media. One dish was placed at RT and one at 4 °C to slow down the embryo development. For the micro-injection procedure, 15–20 zygotes were taken from the Petri dish at RT and placed on a glass depression slide. The Petri dish at RT was then moved at 4 °C, while the other one was moved from 4 °C to RT for the next round of micro-injection. This alternating pattern was continued for subsequent rounds until all the embryos were micro-injected.

The glass slide with zygotes was placed on a cooling stage at 12 °C located on a Nikon Eclipse Ti2 inverted microscope equipped with Eppendorf TransferMan 4r micromanipulators. The cooling stage increased the rigidity of the embryos. Micro-injection was performed using a 20× objective and DIC optics. Embryos were held in place with a standard holding pipette made from borosilicate glass (Harvard Apparatus #GC100-15). Holding pipettes were pulled with a Sutter Horizontal needle puller P-87, flame polished with a Narishige microforge, and connected to an Eppendorf CellTram 4r Air pneumatic syringe. The holding pipette kept the embryos still and facilitated pulling the needle out. Embryo injections were performed using glass needles made from borosilicate glass capillaries containing an internal filament (Harvard Apparatus #GC100TF-10) fashioned with a Sutter Horizontal needle puller P-87 and backfilled by capillary pressure. The tip of the glass needle was gently opened using the edge of the holding pipette. Too small/sharp of a tip will result in immediate lysis of the embryos while too dull of a tip will not allow the needle to penetrate the cell membrane.

Micro-injection pressures were controlled with an Eppendorf FemtoJet 4i (compensation pressure 20–30 hPa, injection pressure 90–100 hPa). Additionally, the WPI MICRO-ePORE pinpoint cell penetrator electroporation device was incorporated into the micro-injection procedure (frequency 520 Hz, amplitude 0.480 V). The MICRO-ePORE reduced the mechanical stress of the micro-injection. Following micro-injection, the embryos were moved from the slide to a new Petri dish with 5% FBS in Embryo Media and stored at RT.

To test for micro-injection efficiency, we injected 2 mg/ml 3 kDa Dextran Texas Red (Thermo Fisher Scientific #D3329) and 0.05% Phenol Red (Sigma #P0290) in diH_2O.

To synthesize exogenous mRNA, we amplified the constructs of interest through PCR with Phusion High-Fidelity DNA Polymerase (NEB #M0530), we purified the PCR product, we performed in vitro transcription using the mMESSAGE mMACHINE High Yield Capped RNA Transcription Kit (Invitrogen #AM1344 or #AM1348) following the manufacturer's protocols, we used the Poly(A) Tailing Kit (Invitrogen #AM1350) and we purified the synthesized mRNA with the MEGAclear Transcription Clean-Up Kit (Invitrogen # AM1908). After quantifying the mRNA using the Qubit® 2.0 Fluorometer (Invitrogen), we micro-injected the embryos with 75 ng/ul exogenous mRNA and 0.05% Phenol Red in diH_2O.

The dividing embryos were cultured *ex ovo* using the ePVF aliquots that passed the contamination and quality test. After 11–13 days in *ex ovo* culture, the embryos were moved in a Petri dish in Hatchling Media (1 mg/ml galactose and 1 mM $CaCl_2$ in Embryo Media). After 3–5 days the snails were moved in Juvenile Media (1 mM $CaCl_2$ in Embryo Media) and fed with small pieces of salad and after 7–10 days they were moved in system water.

Fluorescent in situ hybridization (HCR)

After collecting the tissue of interest as already mentioned, we fixed the samples in 4% PFA with 0.1% Tween 20 at 4 °C ON on a rotator. After fixation, the samples were incubated twice in PBSTx 0.5% over 20 min, then, in pre-heated reduction solution (1% NP40 or IGEPAL, 0.5% SDS in 1x PBS; 50 mM DTT was added only before use) at 37 °C for 15 min, twice in PBSTx 0.5% over 20 min, in 50% MeOH in diH_2O for 10 min and in 100% MeOH for 10 min. Finally, the samples were stored in clean 100% MeOH at −20 °C.

To re-hydrate and bleach the samples, we incubated them in 50% MeOH in diH_2O for 10 min, in PBSTw 0.5% for 10 min, twice in 0.5% Tween 20 in diH_2O over 10 min, in 80% acetone in diH_2O for 30 min at −20 °C, four times in PBSTx 2% for 30 min and finally in bleaching solution (6% H_2O_2 in PBSTx 0.5%) under direct light. To store the samples, we repeated the washes and dehydration steps already performed after the PFA fixation.

Fluorescent in situ hybridization chain reaction (HCR) v3[94] was performed based upon Molecular Instruments' RNA-FISH generic samples in solution protocol. If the samples are too small to settle by gravity, we centrifuged at 500 × *g* for 10 s. Samples were processed in 1.7 ml or 2 ml tubes that were positioned horizontally and allowed to rock gently during all incubations and washes.

HCR was performed on *pax6*-B5 (LOC112559942), *rhodopsin*-B4 (LOC112576458) and *nec2*-B2 (LOC112570448) (Molecular Instruments) and the amplifiers used were B2-488, B4-546, B5-488 and B5-647 (Molecular Instruments).

Immediately prior to imaging, samples were cleared in OptiPrep (Iodixanol) (Sigma #D1556) for 30–60 min at RT and then mounted in ProLong Glass Mountant (Thermo Fisher Scientific #P36980) between two coverslips separated by vacuum grease. Images were acquired with a Nikon CSU-W1 Ti2-E Spinning Disk confocal microscope or with a Zeiss 980 laser scanning microscope with Airyscan 2. After image acquisition, Fiji software[68] was used for exporting and processing images.

Stable mutant lines through CRISPR-Cas9

Genomic locations of interest were evaluated for potential guideRNA (gRNA) target sites using CCTop[95]. The resulting sites were assessed using the predicted on-target efficiency score and the off-target potential[96]. The gRNA had to rank medium or high from CCTOP and target a location downstream of the start site and inside of an exon (see

Supplementary Data 5). The sequences were ordered as Alt-R CRISPR-Cas9 crRNA from Integrated DNA Technologies (IDT). Five ul of 500 ng/ul crRNA was hybridized with 10 ul of 500 ng/ul universal tracrRNA (IDT) at 95 °C for 5 min and then cooled to RT to form a full-length gRNA. The ribonucleoprotein (RNP) complex was prepared by mixing 1 ul of 500 ng/ul hybridized cr/tracrRNA with 0.5 ul of 1 ug/ul Cas9 protein HiFi V3 (IDT), incubating at RT for 20 min, cooling on ice for 20 min and then adding 43.5 ul of diH_2O and 5 ul of 0.5% Phenol Red (Sigma #P0290). The injection mix was centrifuged at 20,000 × *g* for 5 min at 4 °C and then the top 35 ul were recovered in a new tube. The final injection mix composition was 10 ng/ul hybridized cr/tracrRNA, 10 ng/ul Cas9 protein HiFi V3 and 0.05% Phenol Red in diH_2O stored on ice until use.

Embryos were micro-injected, *ex ovo* cultured and grew to adults as already mentioned. Some F0s were genotyped to evaluate the gRNA activity and efficiency of this technology on apple snails. Other F0s were in-crossed with each other or out-crossed with wild-type snails. F1s from each cross were genotyped and then selected F1s were in-crossed to obtain F2s. Finally, to maintain the lines, F1s were out-crossed with wild-type snails and the offspring was genotyped and selected based on presence of indels.

To genotype apple snails, whole F0 or F1 embryos or tips of tentacles were lysed in 50 ul of QuickExtract™ DNA Extraction Solution (Epicentre #QE09050) and processed as suggested by the manufacturer (65 °C for 6 min and 98 °C for 2 min). PCR was performed (98 °C for 30 s; 30 times 98 °C for 10 s, annealing temp. for 10 s, 72 °C for 10 s; 72 °C for 2 min) to amplify the specific genomic location, followed by a second round of amplification to incorporate sample-specific dual barcodes (see Supplementary Data 5). Each PCR reaction was set up with 5 ul NEB Next enzyme (New England BioLabs), 1 ul of lysed tissue and 0.5 uM of each primer. All amplicons were pooled and size-selected using ProNex Size-Selective Purification System (Promega #NG2001). The quantity and quality of cleaned pools were determined by the Qubit® 2.0 Fluorometer (Invitrogen) and Agilent 2100 Bioanalyzer (Agilent Technologies), respectively. Purified pools were run on an Illumina MiSeq 250 flow cell. The resulting sequence data was demultiplexed, and read pairs were joined. On-target indel frequency and expected mutations were analyzed using CRIS.py[97].

Embryo phenotype analyses

To evaluate phenotypes, embryos were harvested at the desired stage as already mentioned. They were mounted on a slide using 2% methylcellulose in Embryo Media and imaged with a Leica M205 FA stereomicroscope equipped with a Leica DFC310 FX camera. After image acquisition, Fiji software[68] was used for exporting and processing images.

Embryos were also fixed in 4% PFA at 4 °C ON, washed four times in PBSTx 2% over 2 h, washed twice in PBSTx 0.5% over 10 min and incubated in 1:400 AlexaFluor488-Phalloidin (Invitrogen #A12379) in PBSTx 0.5% for 2 h at RT. We washed the samples three times in PBSTx 0.5% over 15 min, incubated in 1:1000 DAPI in PBSTx 0.5% and rinsed once in 1x PBS. After washing the embryos twice in 1x PBS, we mounted them on glass bottom Petri dishes using 1% low melting point agarose in Embryo Media and acquired confocal images using the Nikon CSU-W1 Ti2-E Spinning Disk confocal microscope. After image acquisition, Fiji software[68] was used for exporting and processing images.

The homozygous mutant embryos were manually hatched, raised for 2 months in 1 mg/ml galactose Embryo Media replaced daily and manually hand-fed lettuce for all their life.

Statistical analysis

All statistical tests were performed using GraphPad Prism 9 (version 9.4.1). Normal distribution was assessed using Kolmogorov–Smirnov test. Statistical significance was calculated using either one-way ANOVA with Tukey's post hoc multiple comparisons test or non-parametric Kruskal–Wallis ANOVA with Dunn's post hoc multiple comparisons test. *p* values smaller than 0.05 were considered statistically significant. Plots were made in GraphPad Prism 9.

Reporting summary

Further information on research design is available in the Nature Portfolio Reporting Summary linked to this article.

Data availability

Original data underlying this manuscript can be accessed from the Stowers Original Data Repository at http://www.stowers.org/research/publications/libpb-2417. Eye regeneration RNA-Seq data have been deposited at GEO with accession number GSE240085. Tissue-specific RNA-Seq dataset was previously deposited as a GEO Series with accession number PRJNA473253. Processed data are available at https://github.com/AliceAccorsi/SnailEyeRegeneration and in the release https://doi.org/10.5281/zenodo.15635009. Any additional information required to reanalyze the data reported in this paper is available upon request.

Code availability

All original code is available in GitHub at https://github.com/AliceAccorsi/SnailEyeRegeneration and in the release https://doi.org/10.5281/zenodo.15635009. Any additional information required to reanalyze the data reported in this paper is available upon request.

References

1. Sánchez Alvarado, A. & Tsonis, P. A. Bridging the regeneration gap: genetic insights from diverse animal models. *Nat. Rev. Genet.* **7**, 873–884 (2006).
2. Srivastava, M. Beyond Casual Resemblance: Rigorous Frameworks for Comparing Regeneration Across Species. *Annu. Rev. Cell Dev. Biol.* **37**, 415–440 (2021).
3. Fernald, R. D. Casting a Genetic Light on the Evolution of Eyes. **313**, 1914-1918 (2006).
4. Nilsson, D.-E. Eye evolution and its functional basis. *Vis. Neurosci.* **30**, 5–20 (2013).
5. Land, M. F. & Nilsson, D.-E. *Animal eyes* (Oxford University Press, 2012).
6. Lapan, S. W. & Reddien, P. W. Transcriptome analysis of the planarian eye identifies ovo as a specific regulator of eye regeneration. *Cell Rep.* **2**, 294–307 (2012).
7. Wan, J. & Goldman, D. Retina regeneration in zebrafish. *Curr. Opin. Genet. Dev.* **40**, 41–47 (2016).
8. Kha, C. X., Guerin, D. J. & Tseng, K. A.-S. Using the xenopus developmental eye regrowth system to distinguish the role of developmental versus regenerative mechanisms. *Front. Physiol.* **10**, 502 (2019).
9. Tsissios, G. et al. Macrophages modulate fibrosis during newt lens regeneration. *Stem Cell Res. Ther.* **15**, 141 (2024).
10. Islam, M. D. R. et al. The newt reprograms mature RPE cells into a unique multipotent state for retinal regeneration. *Sci. Rep.* **4**, 6043 (2014).
11. Spallanzani, L., Dalyell, J. G. & Bonnet, C. *Tracts on the natural history of animals and vegetables.* (eds Creech, W. and Constable, A.) (1803)
12. Bever, M. M. & Borgens, R. B. Eye regeneration in the mystery snail. *J. Exp. Zool.* **245**, 33–42 (1988).
13. Tuchina, O. & Meyer-Rochow, V. B. Regeneration of the visual system in gastropods (Mollusca). *Invertebr. Biol.* **129**, 27–38 (2010).
14. Tartakovskaya, O. S., Borisenko, S. L. & Zhukov, V. V. Role of the age factor in eye regeneration in the gastropod Achatina fulica. *Biol. Bull. Russian Acad. Sci.* **30**, 228–235 (2003).
15. Sánchez Alvarado, A. To solve old problems, study new research organisms. *Dev. Biol.* **433**, 111–114 (2018).

16. Estebenet, A. L. & Martín, P. R. Pomacea canaliculata (Gastropoda: Ampullariidae): Life-history Traits and their Plasticity. *Biocell* **26**, 83–89 (2002).
17. Guo, L. et al. An adaptable chromosome preparation methodology for use in invertebrate research organisms. *BMC Biol.* **16**, 25 (2018).
18. Sun, J. et al. Signatures of divergence, invasiveness, and terrestrialization revealed by four apple snail genomes. *Mol. Biol. Evol.* **36**, 1507–1520 (2019).
19. Liu, C. et al. The genome of the golden apple snail Pomacea canaliculata provides insight into stress tolerance and invasive adaptation. *Gigascience* **7**, giy101 (2018).
20. Zhou, X. et al. The complete mitochondrial genome of Pomacea canaliculata (Gastropoda: Ampullariidae). *Mitochondrial DNA A DNA Mapp. Seq. Anal.* **27**, 884–885 (2016).
21. Arendt, D. Evolution of eyes and photoreceptor cell types. *Int. J. Dev. Biol.* **47**, 563–571 (2003).
22. Morshedian, A. & Fain, G. L. The evolution of rod photoreceptors. *Philos. Trans. R. Soc. Lond. B Biol. Sci.* **372**, 20160074 (2017).
23. Irwin, A. R., Williams, S. T., Speiser, D. I. & Roberts, N. W. The marine gastropod *Conomurex luhuanus* (Strombidae) has high-resolution spatial vision and eyes with complex retinas. *J. Exp. Biol.* **225**, jeb243927 (2022).
24. Serb, J. M. & Eernisse, D. J. Charting evolution's trajectory: using molluscan eye diversity to understand parallel and convergent evolution. *Evo Edu Outreach* **1**, 439–447 (2008).
25. Gehring, W. J. & Ikeo, K. Pax 6: mastering eye morphogenesis and eye evolution. *Trends Genet.* **15**, 371–377 (1999).
26. Gehring, W. J. The genetic control of eye development and its implications for the evolution of the various eye-types. *Int. J. Dev. Biol.* **46**, 65–73 (2002).
27. Gehring, W. J. New perspectives on eye development and the evolution of eyes and photoreceptors. *J. Heredity* **96**, 171–184 (2005).
28. Buono, L. & Martinez-Morales, J.-R. Retina development in vertebrates: systems biology approaches to understanding genetic programs. *Bioessays* **42**, e1900187 (2020).
29. Ashery-Padan, R., Marquardt, T., Zhou, X. & Gruss, P. Pax6 activity in the lens primordium is required for lens formation and for correct placement of a single retina in the eye. *Genes Dev.* **14**, 2701–2711 (2000).
30. Quinn, J. C., West, J. D. & Hill, R. E. Multiple functions for Pax6 in mouse eye and nasal development. *Genes Dev.* **10**, 435–446 (1996).
31. Davison, A. et al. Formin is associated with left-right asymmetry in the pond snail and the frog. *Curr. Biol.* **26**, 654–660 (2016).
32. Kuroda, R. et al. Diaphanous gene mutation affects spiral cleavage and chirality in snails. *Sci. Rep.* **6**, 34809 (2016).
33. Martín-Durán, J. M., Vellutini, B. C. & Hejnol, A. Embryonic chirality and the evolution of spiralian left–right asymmetries. *Philos. Trans. R. Soc. B* **371**, 20150411 (2016).
34. Grande, C. & Patel, N. H. Nodal signaling is involved in left-right asymmetry in snails. *Nature* **457**, 1007 –1011 (2009).
35. Suetsugu-Maki, R. et al. Lens regeneration in axolotl: new evidence of developmental plasticity. *BMC Biol.* **10**, 103 (2012).
36. Davison, A. & Neiman, M. Mobilizing molluscan models and genomes in biology. *Philos. Trans. R. Soc. Lond. B Biol. Sci.* **376**, 20200163 (2021).
37. Lamb, T. D., Collin, S. P. & Pugh, E. N. Evolution of the vertebrate eye: opsins, photoreceptors, retina and eye cup. *Nat. Rev. Neurosci.* **8**, 960–976 (2007).
38. Koenig, K. M., Sun, P., Meyer, E. & Gross, J. M. Eye development and photoreceptor differentiation in the cephalopod *Doryteuthis pealeii*. *Development* dev.134254 https://doi.org/10.1242/dev.134254 (2016).
39. Knapp, D. & Tanaka, E. M. Regeneration and reprogramming. *Curr. Opin. Genet Dev.* **22**, 485–493 (2012).
40. Becker, C. G. & Becker, T. Growth and pathfinding of regenerating axons in the optic projection of adult fish. *J. Neurosci. Res.* **85**, 2793–2799 (2007).
41. Bobkova, M. V., Tartakovskaya, O. S., Borissenko, S. L., Zhukov, V. V. & Meyer-Rochow, V. B. Restoration of morphological and functional integrity in the regenerating eye of the giant African land snail *Achatina fulica*. *Acta Zoologica* **85**, 1–14 (2004).
42. Hughes, H. P. I. Structure and regeneration of the eyes of strombid gastropods. *Cell Tissue Res.* **171**, 259–271 (1976).
43. Adler, C. E. & Sánchez Alvarado, A. Types or states? Cellular dynamics and regenerative potential. *Trends Cell Biol.* **25**, 687–696 (2016).
44. Özpolat, B. D. & Bely, A. E. Developmental and molecular biology of annelid regeneration: a comparative review of recent studies. *Curr. Opin. Genet Dev.* **40**, 144–153 (2016).
45. Conedera, F. M., Pousa, A. M. Q., Mercader, N., Tschopp, M. & Enzmann, V. Retinal microglia signaling affects Müller cell behavior in the zebrafish following laser injury induction. *Glia* **67**, 1150–1166 (2019).
46. Bergamini, G. et al. Clodronate liposome-mediated phagocytic hemocyte depletion affects the regeneration of the cephalic tentacle of the invasive snail, Pomacea canaliculata. *Biology* **12**, 992 (2023).
47. Nüsslein-Volhard, C. & Wieschaus, E. Mutations affecting segment number and polarity in Drosophila. *Nature* **287**, 795–801 (1980).
48. Solnica-Krezel, L. et al. Mutations affecting cell fates and cellular rearrangements during gastrulation in zebrafish. *Development* **123**, 67–80 (1996).
49. Lawson, N. D. & Wolfe, S. A. Forward and reverse genetic approaches for the analysis of vertebrate development in the zebrafish. *Dev. Cell* **21**, 48–64 (2011).
50. Nairz, K., Zipperlen, P., Dearolf, C., Basler, K. & Hafen, E. A reverse genetic screen in Drosophila using a deletion-inducing mutagen. *Genome Biol.* **5**, R83 (2004).
51. Doudna, J. A. & Charpentier, E. Genome editing. The new frontier of genome engineering with CRISPR-Cas9. *Science* **346**, 1258096 (2014).
52. Momose, T. et al. High doses of CRISPR/Cas9 ribonucleoprotein efficiently induce gene knockout with low mosaicism in the hydrozoan Clytia hemisphaerica through microhomology-mediated deletion. *Sci. Rep.* **8**, 11734 (2018).
53. Ikmi, A., McKinney, S. A., Delventhal, K. M. & Gibson, M. C. TALEN and CRISPR/Cas9-mediated genome editing in the early-branching metazoan Nematostella vectensis. *Nat. Commun.* **5**, 5486 (2014).
54. Ricci, L. & Srivastava, M. Transgenesis in the acoel worm Hofstenia miamia. *Dev. Cell* **56**, 3160–3170.e4 (2021).
55. Crawford, K. et al. Highly efficient knockout of a squid pigmentation gene. *Curr. Biol.* **30**, 3484–3490.e4 (2020).
56. Abe, M. & Kuroda, R. The development of CRISPR for a mollusc establishes the formin Lsdia1 as the long-sought gene for snail dextral/sinistral coiling. *Development* **146**, dev175976 (2019).
57. Perry, K. J. & Henry, J. Q. CRISPR/Cas9-mediated genome modification in the mollusc, Crepidula fornicata. *Genesis* **53**, 237–244 (2015).
58. Sun, D., Guo, Z., Liu, Y. & Zhang, Y. Progress and prospects of CRISPR/Cas systems in insects and other arthropods. *Front. Physiol.* **8**, 608 (2017).
59. Schell, T. et al. An annotated draft genome for Radix auricularia (Gastropoda, Mollusca). *Genome Biol. Evol.* **9**, 0 (2017).
60. Webster, N. B. & Meyer, N. P. Capitella teleta gets left out: possible evolutionary shift causes loss of left tissues rather than increased neural tissue from dominant-negative BMPR1. *Neural Dev.* **19**, 4 (2024).
61. Li, Q., Yu, H. & Li, Q. Dual sgRNA-directed tyrosinases knockout using CRISPR/Cas9 technology in Pacific oyster (Crassostrea gigas)

reveals their roles in early shell calcification. *Gene* **927**, 148748 (2024).
62. Macosko, E. Z. et al. Highly parallel genome-wide expression profiling of individual cells using nanoliter droplets. *Cell* **161**, 1202–1214 (2015).
63. Halder, G., Callaerts, P. & Gehring, W. J. Induction of ectopic eyes by targeted expression of the eyeless gene in Drosophila. *Science* **267**, 1788–1792 (1995).
64. Swaroop, A., Kim, D. & Forrest, D. Transcriptional regulation of photoreceptor development and homeostasis in the mammalian retina. *Nat. Rev. Neurosci.* **11**, 563–576 (2010).
65. van Heyningen, V. & Williamson, K. A. PAX6 in sensory development. *Hum. Mol. Genet.* **11**, 1161–1167 (2002).
66. Klann, M. & Seaver, E. C. Functional role of pax6 during eye and nervous system development in the annelid Capitella teleta. *Dev. Biol.* **456**, 86–103 (2019).
67. Navet, S., Andouche, A., Baratte, S. & Bonnaud, L. Shh and Pax6 have unconventional expression patterns in embryonic morphogenesis in Sepia officinalis (Cephalopoda). *Gene Expr. Patterns* **9**, 461–467 (2009).
68. Schindelin, J. et al. Fiji: an open-source platform for biological-image analysis. *Nat. Methods* **9**, 676–682 (2012).
69. Adler, C. E., Seidel, C. W., McKinney, S. A. & Sánchez Alvarado, A. Selective amputation of the pharynx identifies a FoxA-dependent regeneration program in planaria. *eLife* **3**, e02238 (2014).
70. Nuckolls, N. L. et al. The wtf4 meiotic driver utilizes controlled protein aggregation to generate selective cell death. *eLife* **9**, e55694 (2020).
71. Dobin, A. et al. STAR: ultrafast universal RNA-seq aligner. *Bioinformatics* **29**, 15–21 (2013).
72. Li, B. & Dewey, C. N. RSEM: accurate transcript quantification from RNA-Seq data with or without a reference genome. *BMC Bioinforma.* **12**, 323 (2011).
73. Robinson, M. D., McCarthy, D. J. & Smyth, G. K. edgeR: a Bioconductor package for differential expression analysis of digital gene expression data. *Bioinformatics* **26**, 139–140 (2010).
74. McCarthy, D. J., Chen, Y. & Smyth, G. K. Differential expression analysis of multifactor RNA-Seq experiments with respect to biological variation. *Nucleic Acids Res.* **40**, 4288–4297 (2012).
75. Chen, Y., Lun, A. T. L. & Smyth, G. K. From reads to genes to pathways: differential expression analysis of RNA-Seq experiments using Rsubread and the edgeR quasi-likelihood pipeline. *F1000Res.* **5**, 1438 (2016).
76. Wickham, H. et al. Welcome to the Tidyverse. *JOSS* **4**, 1686 (2019).
77. Thomas, P. D. et al. PANTHER: Making genome-scale phylogenetics accessible to all. *Protein Sci.* **31**, 8–22 (2022).
78. Altenhoff, A. M. et al. OMA standalone: orthology inference among public and custom genomes and transcriptomes. *Genome Res.* **29**, 1152–1163 (2019).
79. Blum, M. et al. The InterPro protein families and domains database: 20 years on. *Nucleic Acids Res.* **49**, D344–D354 (2021).
80. Jones, P. et al. InterProScan 5: genome-scale protein function classification. *Bioinformatics* **30**, 1236–1240 (2014).
81. Marc Carlson, H. P. AnnotationForge. *Bioconductor* https://doi.org/10.18129/B9.BIOC.ANNOTATIONFORGE (2017).
82. Yu, G., Wang, L.-G., Han, Y. & He, Q.-Y. clusterProfiler: an R Package for Comparing Biological Themes Among Gene Clusters. *OMICS A J. Integr. Biol.* **16**, 284–287 (2012).
83. Wu, T. et al. clusterProfiler 4.0: a universal enrichment tool for interpreting omics data. *Innovation* **2**, 100141 (2021).
84. Yu, G. Gene ontology semantic similarity analysis using GOSemSim. In *Stem cell transcriptional networks* (ed. Kidder, B. L.) vol. 2117 207–215 (Springer US, 2020).
85. Wilke, C. cowplot: Streamlined Plot Theme and Plot Annotations for 'ggplot2'. https://wilkelab.org/cowplot/ (2025)
86. Yu, G. enrichplot. *Bioconductor* https://doi.org/10.18129/B9.BIOC.ENRICHPLOT (2018).
87. Reijnders, M. J. M. F. & Waterhouse, R. M. Summary visualizations of gene ontology terms with GO-Figure!. *Front. Bioinform* **1**, 638255 (2021).
88. Letunic, I., Khedkar, S. & Bork, P. SMART: recent updates, new developments and status in 2020. *Nucleic Acids Res.* **49**, D458–D460 (2021).
89. Jumper, J. et al. Highly accurate protein structure prediction with AlphaFold. *Nature* **596**, 583–589 (2021).
90. Mirdita, M. et al. ColabFold: making protein folding accessible to all. *Nat. Methods* **19**, 679–682 (2022).
91. Pettersen, E. F. et al. UCSF ChimeraX: structure visualization for researchers, educators, and developers. *Protein Sci.* **30**, 70–82 (2021).
92. Madeira, F. et al. Search and sequence analysis tools services from EMBL-EBI in 2022. *Nucleic Acids Res.* **50**, W276–W279 (2022).
93. Edgar, R. C. MUSCLE: multiple sequence alignment with high accuracy and high throughput. *Nucleic Acids Res.* **32**, 1792–1797 (2004).
94. Choi, H. M. T. et al. Third-generation in situ hybridization chain reaction: multiplexed, quantitative, sensitive, versatile, robust. *Development* **145**, dev165753 (2018).
95. Stemmer, M., Thumberger, T., Del Sol Keyer, M., Wittbrodt, J. & Mateo, J. L. CCTop: an intuitive, flexible and reliable CRISPR/Cas9 target prediction tool. *PLoS ONE* **10**, e0124633 (2015).
96. Labuhn, M. et al. Refined sgRNA efficacy prediction improves large- and small-scale CRISPR–Cas9 applications. *Nucleic Acids Res.* **46**, 1375–1385 (2018).
97. Connelly, J. P. & Pruett-Miller, S. M. CRIS.py: a versatile and high-throughput analysis program for CRISPR-based genome editing. *Sci. Rep.* **9**, 4194 (2019).

Acknowledgements

We would like to thank Drs. Robb Krumlauf, Stephanie Nowotarski, Julia Peloggia de Castro, Frederick Mann and Viraj Doddihal for critical reading of the manuscript. We also thank the Sánchez Alvarado lab members for insightful discussions; Tonyea Inglis for the support in applying for the apple snail permit; the Stowers Institute for Medical Research (SIMR) Invertebrates Core, Carlos Barradas Chacón and Robert Schnittker for maintaining the *P. canaliculata* colony; Davide Malagoli for providing animals to establish the SIMR apple snail colony; the SIMR Histology Core, Cindy Maddera, the SIMR Genome Engineering core and the SIMR Sequencing Core for experimental assistance; Sofia Robb for OMA support; the Stowers Café for providing lettuce for feeding the snails. The work was funded by Howard Hughes Medical Institute (ASA), Society for Developmental Biology Emerging Models Grant (AA), American Association for Anatomy Postdoctoral Fellowship (AA), by institutional support from the SIMR (ASA) and from UC Davis (AA).

Author contributions

Conceptualization: A.A. and A.S.A.; Methodology: A.A., T.J.C., K.D.; Investigation: A.A., T.J.C., M.M., K.W., A.G., J.M., M.C.M.; Data Analysis: A.A., E.R., B.P., S.A.M.; Writing – original draft: A.A.; Writing – review and editing: A.A., E.R., B.P., T.J.C., M.M., K.W., K.D., J.M., M.C.M., S.A.M., A.S.A.; Funding acquisition: A.A., A.S.A.; Resources: A.A., A.S.A.; Supervision: A.A., A.S.A.

Competing interests

The authors declare no competing interests.

Additional information

Supplementary information The online version contains supplementary material available at https://doi.org/10.1038/s41467-025-61681-6.

Correspondence and requests for materials should be addressed to Alice Accorsi or Alejandro Sánchez Alvarado.

Peer review information *Nature Communications* thanks Victoria Sleight and the other, anonymous, reviewer(s) for their contribution to the peer review of this work. A peer review file is available.